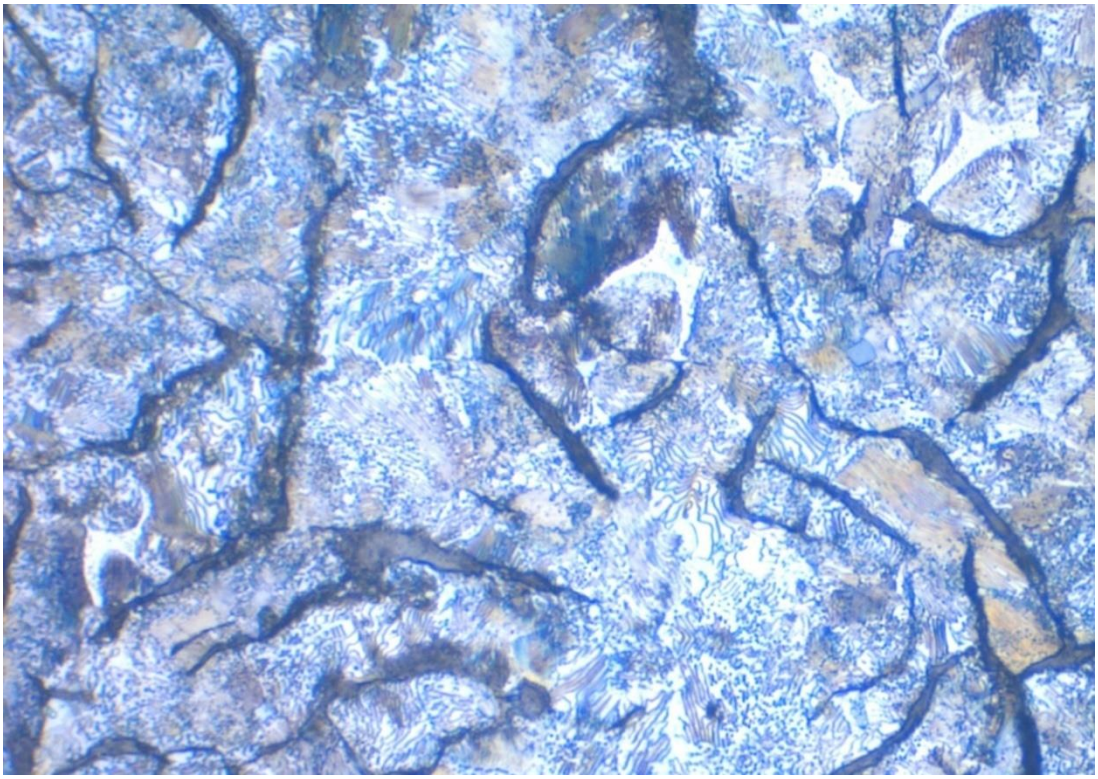

Kantonsschule Im Lee Winterthur

Maturitätsarbeit HS 2022/23

It Just Won't Stick! –

THE EFFECT OF DIFFERENT REAGENTS ON THE NON-STICK PROPERTY OF SEASONED CAST IRON PANS

Deron Ohannes Kurtcuoglu, Class 4a

Supervisor: Raphael Sigrist

Winterthur, 09.01.2023

Table of Contents

Preface

Cooking has been a part of my life for as long as I can remember. But as much as I enjoy cooking, I dislike cleaning up after myself equally. That is why I love non-stick cookware, they make cleaning one's pans so much easier, and save a lot of time.

But I never appreciated it fully, at least not until one day, when we were looking at Van der Waals forces in chemistry class. As an example, for a material that exhibits extremely low Van der Waals forces, we were introduced to Teflon. That is where my fascination with non-stick materials started. To have a substance that practically sticks to nothing, and yet it sticks to itself was fascinating to me.

When it came time to choose the topic of my thesis, I realized that I wanted to investigate low adhesive materials. Yet, instead of looking into Teflon or other cookware, such as ceramic, I decided to study something that has been used for centuries: cast-iron.

I would like to thank the following people for their support throughout this project, without whom none of it would have been possible:

A big thank you to my chemistry teacher, Raphael Sigrist, who always makes classes interesting and was always encouraging in my pursuits of (Teflon-related) knowledge. Without him, I would surely not have tackled the topic at hand.

I owe much gratitude to Prof. Dr. Wendelin Stark for hosting me in his lab at ETH Zurich, and for his valuable advice in the beginnings of the project. A very special thanks to Dr. Olivier Gröninger and Patrik Willi, for answering more questions than I can remember, helping me with my experimental setup and showing me around the lab whenever I couldn't find a dish, chemical or the waste disposal. Thank you also to rest of the lab for never hesitating to assist me when Olivier or Patrik weren't there and for letting me eat lunch with them.

A special thank you also to the central workshop D-CHAB at ETH Zurich, for cutting and sanding the samples.

Thank you also to Prof. Dr. Arne Wahlen for letting me do measurements in his laboratory at the Fachhochschule Nordwestschweiz and blocking literally an entire day out of his busy schedule to help me with them. I still owe him a z'Vieri. A special thank you to Sabine Maass of the FHNW for helping me with the SEM.

A special thank you also to Prof. Dr. Li Cunpu, School of Chemistry and Chemical Engineering, Chongqing University, PR China, for taking time to look over my research protocol and for answering my questions regarding cast-iron seasoning.

I would also like to thank my family for their support, especially my parents, for their advice, help with editing, formatting and statistics, and the lamb tallow I used. Thanks also to my grandfather, for finding the cast-iron griddle I used for the sample plates.

Introduction

A VERY BRIEF HISTORY OF COOKWARE

The act of cooking is deeply engrained in us humans. Some research suggests that we have been cooking for almost 2 million years [1]. The earliest known pottery vessels that are believed to have been used for cooking were found in the Xianrendong Cave in Jiangxi, China, and date back to about 20 000 BP [2].

In terms of metal cookware, brass was long the premier material [3]. In the 17th century, the production of brass utensils was most predominant in the Netherlands, due to superior knowledge of economical production methods. However in 1707, Abraham Darby patented his method of "Casting Iron Bellied Pots in Sand Only" [4]. He had travelled to the Netherlands in 1704, and there discovered what set the local brass cookware production apart from the English: instead of casting in loam and clay, they cast only in sand, making the product smoother and altogether less costly to produce. He went back to England, and realized that he could make the products accessible to more people by using a cheaper material: iron [3].

Additionally, cast iron could be seasoned with a variety of oils and fats to create an anti-corrosion, non-stick coating [5]. However, an alternative to cast iron soon arrived with the invention of PTFE (polytetrafluoroethylene, better known by the brand name Teflon) in 1938 by Roy J. Plunkett, and the introduction of Teflon pans to the public in the 1950s and 60s, with sales becoming larger starting in 1964 [6]. Regardless of the usefulness of Teflon cookware, the production thereof has brought up concerns in past years. The use of various PFAS (per- and polyfluoroalkyl substances), especially PFOA (perfluorooctanoic acid), and their health hazards have been thoroughly documented in the past years [7], [8]. For PFOA, these include kidney cancer, testicular cancer, ulcerative colitis (inflammatory disorder affecting the colon or rectum [9]), thyroid disease, hypercholesterolemia (high cholesterol), and pregnancy-induced hypertension [7], [10].

Although Teflon itself is non-reactive and not toxic up to temperatures of about 260°C, and although PFOA exposure through Teflon cookware is minor, chemical dumps by companies such as DuPont have contributed to the contamination of drinking water, cattle and humans to the extent that an estimated 98% of Americans have PFOA in their blood, albeit in low concentrations [7], [11], [12].

PFOA along with PFOS (perfluorooctane sulfonate) have been phased out in some countries in the past years and are no longer used there in non-stick wares. They have been replaced by other PFAS [13]. Yet, next to the fact that they take a very long time to break down, studies have shown that alternatives to these, such as HFPO-DA (hexafluoropropylene oxide dimer acid) and its ammonium salt (commonly known as GenX), cause some of the same health problems associated with PFOA [13]–[15].

Along with these health concerns comes the problem of durability. Although an average non-stick pan will usually last 3-5 years when used properly, there are many ways to accidentally damage the coating, which reduces the actual usage life span. Due to this short life span, disposal can become an issue [16].

A third downside to Teflon pans is that it they are not only hydrophobic, but that they also repel oil well, which is suboptimal for the cooking process. Instead of spreading out,

oil forms pools, which prevents even heat distribution and, in the end, can make it harder to cook certain foods [17].

This is where the project reported on herein came into play: To combat the problems of pollution and sustainability in conventional non-stick pans, an older and well-known material for cooking ware was investigated, namely cast iron. The goal is to investigate the seasoning process further, so that the understanding thereof can be used to improve the natural non-stick coating of cast iron pans and supply a better alternative to PTFE.

As the starting point to the project, the research paper "Seasoning Chinese cooking pans: The nanoscience behind the Kitchen God's blessing" [17] was used as a reference. Seasoning refers to the process of creating a coating on cookware by overheating a small amount of well-distributed fat or oil on the cooking surface. Several reagents (tallows and fatty acids) were used to season cast iron samples. The seasoning process was conducted with different amounts of reagent and with varying numbers of incubation cycles. Contact angle measurements of water drops on the samples were made to assess hydrophobicity.

BASIC PROPERTIES OF HYDROPHOBIC MATERIALS

Before getting into the seasoning process of cast-iron pans in more detail, it is essential to understand the fundamentals of hydrophobic materials. In the study of surface properties of a material, hydrophobicity describes the ability of the substance to repel water [18]. The action of water or any liquid spreading out on a surface is called wetting. One of the most common approaches to quantifying hydrophobicity is to assess the degree of wetting. This can be done by observing the contact angle at the interface of a water drop on the surface to be characterized [19]:

A drop of water placed on the surface of a material, assuming it does not wet the surface completely, will form a boundary between the solid surface, the surrounding gas (generally air), and the liquid water itself. This is called the three-phase line. The contact angle is defined as the angle between the surface and the tangent to the droplet at the three-phase line (Fig. 1). A categorization for wetting according to the contact angle (θ) of water to a surface can be made as follows [19]:

- θ is $\geq 90°$: The surface is hydrophobic, and the conditions are said to be non-wetting.
- $0 < \theta < 90°$: The surface is hydrophilic and partial wetting conditions are in place.
- $\theta = 0°$: The waterdrop has completely wetted the surface of the material, hence complete wetting conditions apply.
- $\theta > 150°$: The surface is superhydrophobic.

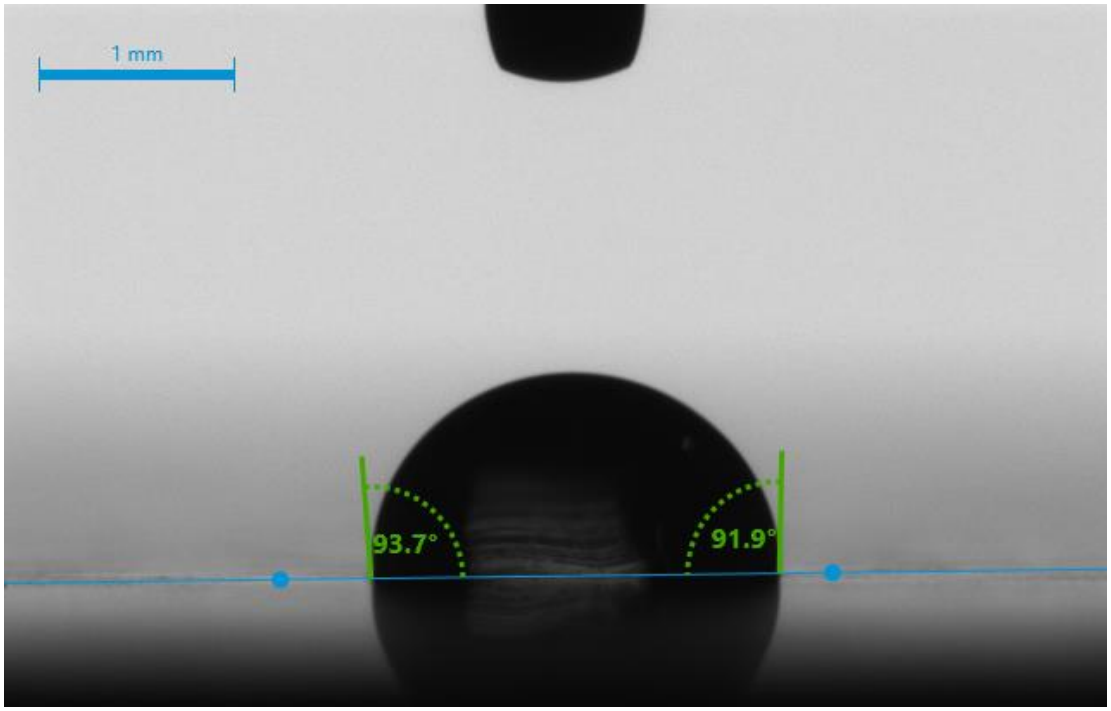

Fig. 1: Photograph illustrating contact angle measurement. A water drop on a surface (Sample 1, see Methods section) is shown, along with the horizontal axis (blue with two dots) representing the plane, the tangents at the three-phase line and the angle (solid green), and the arc of the angles (dotted green). Further, the image scale (top left) and the needle used to place the water drop on the surface (top centre) are visible.

There are two main aspects that influence the contact angle: the surface finish and surface energy of the material in question [20]–[22]. To understand the surface energy, one must first look at chemical bonds in general: Atoms form bonds with one another to reach lower states of energy in total than they would have alone. When a bond is formed, the difference in energy between the single atoms and the newly formed compound is released [23].

Likewise, energy is released into the system when the molecules in the bulk of a substance attract each other. The stronger the attractions, the more energy is released [24]. Assuming a lattice of a given material, an atom in the centre of the lattice can interact with the rest of the material in every direction. This is visualized in Fig. 2 with the central blue sphere forming six connections, each representing a bond (assuming the sixth connection pointing towards the viewer is invisible). One bond points towards one face of the lattice. The atoms at the surface of the material form fewer bonds and, therefore, will have higher energies than the ones in the centre. This surplus of energy at the surface compared to the bulk of the material is called the surface energy [25].

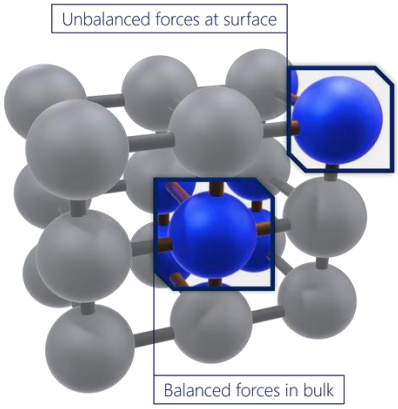

Fig. 2: Illustration of the bonding forces in the bulk and at the surface of a material. Spheres represent single molecules, atoms, or ions. Blue sphere in centre of image represents the conditions within the bulk of the material, hence all possible bonds were formed (bond pointing in direction of viewer was removed for better visibility). Blue sphere in upper right corner of the image represents the conditions at the surface of the material, hence only three of six possible bonds were formed. Source: https://www.ossila.com/en-eu/pages/a-guide-to-surface-energy

The surface, however, will tend to minimize its energy, as it is less energetically favourable for a particle to be at the surface than in the bulk of a material [25]. A nice example to visualize this can be found in drops of water. A common picture seen from the International Space Station ISS is that of an astronaut observing large bubbles of water floating in air (Fig. 3). A direct consequence of the micro-gravity environment is the spherical shape of the water. Since the drop is not forced onto a surface by gravity, the only interface is between the water droplet and the air, creating equal interaction conditions for the whole surface. The reason the water takes on the described form is as follows: Since a surface will tend to minimize its energy, a free-flowing liquid such as water can simply adjust its shape to minimize its surface area [26]. The sphere happens to be the shape with the lowest surface area per volume, so the water will be found in that form when free-floating in zero gravity [26].

Solids, however, cannot freely change their shape the way liquids can. But the surface of a solid can still lower its surface energy. It does so by attracting, or adsorbing another substance, in our case a liquid, onto itself. Depending on the surface energies of the two phases, the solid will be wetted by the liquid to a different degree [27].

Assuming a drop of water is placed on a non-coated copper pan, this drop will spread out, because the surface energy of the solid is much larger than that of water [28]. The relation between wetting level, surface energy (solid) and surface tension (for liquids, surface energy density and surface tension are identical), on an ideal, completely smooth surface, is given by Youngs equation [21], [25]:

$$\sigma s \; = \; \sigma sl \; + \; \sigma l \, cos \, (\theta),$$

where σs is the surface energy, σsl is the interfacial tension, σl the surface tension of the liquid, and cos(θ) the cosine of the contact angle [27].

If Teflon is chosen instead of a copper pan, and a drop of water is placed on it, it will not spread out as much. This is because Teflon's surface energy is that much lower than that of water [28]. However, if Teflon and, e.g., hexane are used, the hexane will spread out more than water, because its surface energy is lower than that of water [28]. This principle can be applied when looking for new hydrophobic materials, since the surface energy is directly linked to the wettability of a surface.

Fig. 3: Picture of astronaut Karan Nyberg with a water bubble in zero gravity. The bubble exhibits its characteristic surface energy minimizing shape under the described conditions, namely a sphere. Photograph by NASA, released to the public domain.

Surface roughness

A further aspect that influences the wettability of a material is the surface roughness. There are two major models for characterizing wettability on rough surfaces, namely the Wenzel model, which assumes a drop of water that is in full contact with the given rough surface, and the Cassie-Baxter model, which describes a drop resting only on the peaks of a rough surface (Fig. 4) [20]–[22].

Wenzel model

The contact angle on a completely smooth surface is given by Young's equation (intrinsic contact angle). The contact angle according to the Wenzel model is then determined by [21], [22]:

$$\cos\theta_w = R_f \cos\theta_0,$$

where θ_w is the contact angle in the Wenzel state and θ_o is the intrinsic contact angle. R_f is the roughness parameter and is given by [22]

$$R_f = \frac{Actual\ area}{Projected\ area}$$

Since the roughness of a surface can always be assumed to be greater than 1, we can draw the following from the equation:

$$|\cos\theta_w| > |\cos\theta_0|$$

This in turn means that for drops with a θ_o smaller than 90°, θ_w will be smaller than θ_o. If θ_o is larger than 90°, θ_w will be larger than θ_o [22].

Cassie-Baxter model

The relation between contact angle of a drop on a rough surface in the Cassie-Baxter state and the intrinsic contact angle can be described by the following equation [20], [21]:

$$\cos\theta_{CB} = f_s(\cos\theta_0 + 1) - 1 \ ,$$

where θ_{CB} is the contact angle of the droplet in the Cassie-Baxter state, f_s is the fraction of the area of the droplet in contact with the solid surface, and θ_o is the intrinsic contact angle [20].

From the equation, the following conclusion can be drawn: As f_s approaches 0, the right side of the equation approaches -1, which means that θ_{CB} approaches 180°. Therefore, in the Cassie-Baxter state, the apparent contact angle θ_{CB} can be larger than 90°, even if the intrinsic contact angle of a drop on a completely smooth version of the given surface is lower than 90°. So, intrinsically hydrophilic surfaces can exhibit hydrophobicity, depending on the surface roughness and the state of the drop on it [20].

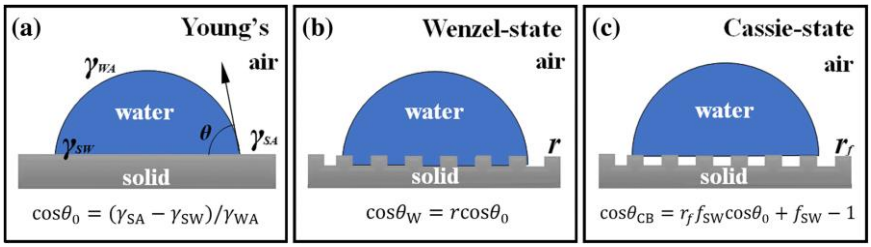

Fig. 4: Illustration comparing the state of a drop on an ideal surface (panel a), the Wenzel-state (panel b), and the Cassie-state (panel c) [29].

THE PROCESS OF SEASONING CAST IRON

Cookware seasoning

To season cookware, for example a pan, a small amount of fat or oil is applied to the clean pan, and the cookware is placed on a stove and heated to the point where the fat or oil exceeds its smoking point. This process is repeated multiple times to form a hydrophobic coating on the cookware.

Process, mechanism and surface behaviour

The process involved and the mechanisms at play when seasoning cast iron are described in the research paper by Gao and co-workers [17]. In the following, their approach is summarized, as it was used as the basis of the current project. Their interpretation of the surface behavior after seasoning is also described.

Process

For their research on cast-iron seasoning, Gao et al. used a muffle furnace instead of an open flame, and their cast-iron pan of choice (Supor FC32E2) was cut into pieces to produce smaller samples [17].

They applied beef tallow to the samples. The samples were subdivided into 5 groups, each according to the temperature they were heated up to, namely 300 °C, 375 °C, 450 °C, 525 °C, and 600 °C. When samples were heated up to temperatures higher than 375°C, an X-ray diffraction analysis (XRD spectra) showed Fe_3O_4 peaks. The increased Fe^{3+} content was additionally verified by X-ray photoelectron spectroscopy (XPS).

The samples were heated up from room temperature to the target temperature at a rate of 5°C/min, and they were incubated at the target temperature for 15 min. The process was repeated in a fashion to where for each group there was one sample for each number of treatment cycles. Concretely, there was one sample Fe-450-1 (heated once to 450°C), one sample Fe-450-2 (heated twice to 450°C) up to cycle 5. This process was done for each target temperature. The resulting contact angle of water on sample Fe-450-5 were measured to be 117.6°, therefore the surface of the sample can be characterized as hydrophobic.

Mechanism

According to Gao et al., the oxygen partial pressure (PO_2) in the region close to the surface increases through the evaporation of the applied fat [17]. Under low PO_2, the iron atoms tend to be in an octahedral coordination and a tetrahedral coordination at high PO_2. Before heating, the iron atoms will be mainly in octahedral coordination. But, as the partial gas pressure of oxygen increases with the heating, the coordination of the iron atoms will change to tetrahedral. This causes the unit cell, the smallest repeating unit within a crystal lattice, to increase in volume by ca. 27% after the inclusion of the oxygen atoms. This expansion of the volume forces the Fe_3O_4 out of the surface. Throughout the cycles, when tallow is applied and low PO_2 conditions apply, the atoms will go back to the octahedral coordination and the volume will decrease. Then, during heating, through increase in PO_2, the iron atoms go into tetrahedral coordination again, and the volume grows larger. This repeated shrinking and growing of the volume breaks the large Fe_3O_4 particles apart into Fe_3O_4 nanoballs [17].

Surface behaviour

According to Gao et al., the Fe_3O_4 nanoballs are intrinsically hydrophobic [17]. So, to describe the fact that this rough surface still exhibits hydrophobic properties, one might assume that the Cassie-Baxter model should be used. However, Gao et al. found that said model was not appropriate when applied to spherical surfaces. Instead they proposed “conditional hydrophobicity” for the surface:

Assuming a drop of water is placed on a nanoball with an intrinsic contact angle <90°, the contact angle between the tangent to the surface of the solid and the tangent to the surface of the liquid (Fig 5: $\theta_{a,o}$) at the three-phase line will also be < 90°. However, the angle between the plane on which the three-phase line rests on and the tangent to the surface of the liquid at the contact line (Fig 5: θ_a) will be larger than $\theta_{a,o}$. If this angle becomes larger than 90 degrees, the surface will appear hydrophobic. There is, however, a limit to the size of the drop. When that limit is reached, the drop will collapse and wet the entire surface. This is how the conditional hydrophobicity was defined [17].

Certain properties that are of advantage during cooking were attributed by Gao et al. to the surface behaviour of the seasoned cast iron pan: If one were to cook a steak in the pan, due to its high water-content, it will have a high level of contact. This allows an efficient transfer of heat from the pan and oil to the surface of the meat, cooking the steak and trapping the rest of the water inside. As the water content at the surface of the meat decreases, so will the level of contact between the steak and the pan, slowing down the heat transfer and preventing the steak from burning.

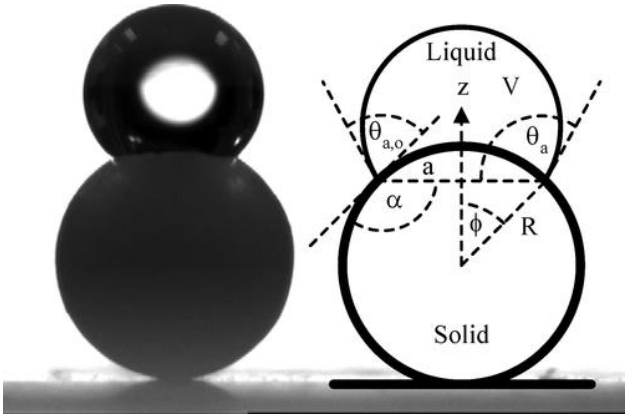

Fig. 5: Picture and illustration of a water droplet on a solid spherical surface. $\theta_{a,0}$ denotes the contact angle between the tangent to the surface of the solid and the tangent to the surface of the liquid. The apparent hydrophobicity is illustrated by θ_a, which shows the angle between the plane on which the three-phase line rests on and the tangent to the surface of the liquid at the contact line [30].

Methodology

TALLOW PRODUCTION

The lamb tallow was produced by rendering lamb fat in a pressure cooker (Instant Pot Duo). Rendering involves cutting the fat into pieces and heating it up, to where the fat is melted [5]. Impurities were removed by straining the molten fat through a fine-meshed metal sieve. The resulting purified liquid fat was left to solidify in the fridge.

SAMPLE PREPARATION

Four experiment series were done, each following the basic principles outlined in the research paper of Gao et al. [17]. In addition, two control samples were prepared. Square cast-iron sample plates of two sizes, roughly 25 cm^2 and ca. 3.125 cm^2 were used. The smaller sample size was introduced later in the study to accommodate size requirements for the quick-loading feature of the SEM (see results), although this proved to be unnecessary. The plates were cut from a grill griddle (Gonser, Grillplatte Gusseisen 36.5 x 20 cm) [31], and the original surface was sanded down completely.

The sample plates were covered with different types and amounts of animal tallow and fatty acids. Two tallows were used: lamb tallow, which was homemade (see tallow production), and commercial beef tallow (Mahler und Co., Brox Rindertalg zum Kochen) [32]. Four fatty acids were used, namely myristic acid, oleic acid, stearic acid, and palmitic acid.

The tallow application was performed as follows:

1. The samples were cleaned with ethyl acetate, ethanol, and a paper towel.
2. Compressed air was used to remove any paper residue.
3. Before each tallow application, the samples were weighed.
4. The tallow was spread as evenly as possible on the samples using disposable spatulas.
5. The samples were weighed again, and if the weight did not correspond to the targeted tallow amount the last step was repeated.

The process for the application of the fatty acids was identical for the first 3 steps. After the third step, instead of applying the fatty acids directly with a spatula, the myristic, stearic and palmitic acid had to be heated up directly on the sample using a heating plate, due to them being solid at room temperature. Once the chemicals melted, they were spread about with the spatula. After the application, the samples were weighed again, as with the tallow, and if necessary, the application was repeated. For oleic acid, steps 1-3 and the weighing at the end were also identical, but the chemical was pipetted directly onto the sample and spread around, due to it being liquid at room temperature.

Subsequently, the sample plates were placed in a furnace (Nabertherm) and heated at a rate of 5°C/min to 450°C, whereafter they were incubated at 450°C for 15 min and taken out of the furnace and left to cool at room temperature.

Series 1

The first experimental series encompassed 5 samples, each having lamb tallow spread on them with amounts averaging between 20 and 30 mg per sample (roughly 1 mg/cm^2). The point of this series was to observe the difference between number of cycles, hence, after each cycle one sample was removed.

Table 1

		Sample				
		1	2	3	4	5
Weight raw sample [g]		41.252	41.144	45.264	40.643	41.131
Amount of tallow added [mg]	**Cycle**					
	1	8	26	28	23	20
	2	12	23	23	15	-
	3	21	34	34	-	-
	4	32	26	-	-	-
	5	38	-	-	-	-
Mean amount of tallow added per cycle [mg]		22	28	27	19	20
Total weight of sample at final cycle [g]		41.262	45.272	41.155	40.650	41.136

Weight measurements for first experimental series. Five samples were tested, each with different number of heating cycles. All samples were surface treated with lamb tallow before each heating cycle.

Series 2

The second experimental series used 3 samples, once again using lamb tallow, but with, respectively, 40, 60 and 80 mg of lamb tallow (ca. 1.5 mg/cm², 2.5 mg/cm², 3 mg/cm²). Each of them underwent 5 cycles at 450°C. The amount of tallow in the third cycle was not measured, because the measurement was overlooked. The goal of this series is to have a comparison of how the weight of applied tallow effects the contact angles.

Table 2

		Sample		
		6	7	8
Weight raw sample [g]		41.570	40.639	41.927
Amount of tallow added (mg)	**Cycle**			
	1	41	62	76
	2	39	59	77
	3	-	-	-
	4	36	68	83
	5	47	59	80
Mean amount of tallow added per cycle [mg]		41	62	79

Weight measurements for experimental Series 2: All samples underwent 5 cycles at 450°C and were coated with different amounts of lamb tallow. For the calculation of the mean amount of tallow, cycle 3 was excluded due to missing data.

Series 3

Experimental Series 3 used three samples, this time with beef tallow. The samples had, respectively, 20, 60 and 80 mg of tallow applied (ca. 1.5 mg/cm², 2.5 mg/cm², 3 mg/cm²). Each plate underwent 5 cycles at 450°C.

Table 3

		Sample		
		9	10	11
Weight raw sample [g]		42.390	33.823	37.446
Amount of tallow added [mg]	**Cycle**			
	1	18	52	70
	2	23	48	84
	3	18	63	85
	4	19	57	76
	5	22	67	83
Mean amount of tallow added per cycle [mg]		20	57	80
Total weight of sample at final cycle [g]		42.403	33.838	37.457

Weight measurements for experimental Series 3: All samples underwent 5 cycles at 450°C and were coated with different amounts of beef tallow.

Series 4

Experimental Series 4 used four samples coated with different fatty acids, namely myristic acid (Sample 18), oleic acid (Sample 19), stearic acid (Sample 20), palmitic acid (Sample 21). It is the first series using the smaller sample plates (≈ 3.125 cm^2).

The amount of the reagent was chosen to have a comparison between Series 2, 3 and 4. More precisely, to compare the Samples 8 and 11 with Series 4, because they each have approximately the same amount of reagent per area. (80 mg/25 cm^2 = 10 mg/3.125 cm^2)

Table 4

		Sample			
		18	19	20	21
Weight raw sample [g]		5818	5968	5878	5934
Amount of tallow added [mg]	**Cycle**				
	1	9	10	11	10
	2	10	10	9	10
	3	10	10	10	9
	4	10	10	10	10
	5	10	10	10	10
Mean amount of tallow added per cycle [mg]		10	10	10	10

Weight measurements for experimental Series 4: All samples underwent 5 cycles at 450°C and were coated with different fatty acids (approximately 3 mg/cm^2)

CONTROLS

Three controls were used for the contact angle measurement and/or surface roughness measurement, Controls B, C and D.

Control B was placed in the furnace for 5 cycles, and heated up to 450°C, without the application of a reagent. Controls C and D were not treated.

Materials

To analyse the type of cast iron that was used, two samples underwent metallography, namely Control B and a sample with the griddles original surface. First, the samples were cut into smaller pieces. Then, plastic clamps were placed onto them to ensure stability,

and they were embedded in a resin with a Struers CitoPress-1. This resulted in a resin cylinder with the samples flush on one surface. The cylinder was then polished using a Struers Tegrapol-21. Subsequently, the samples were etched using Nital (100 ml ethanol (96%) and 2 ml nitric acid). Then, the cross sections were viewed under a light microscope.

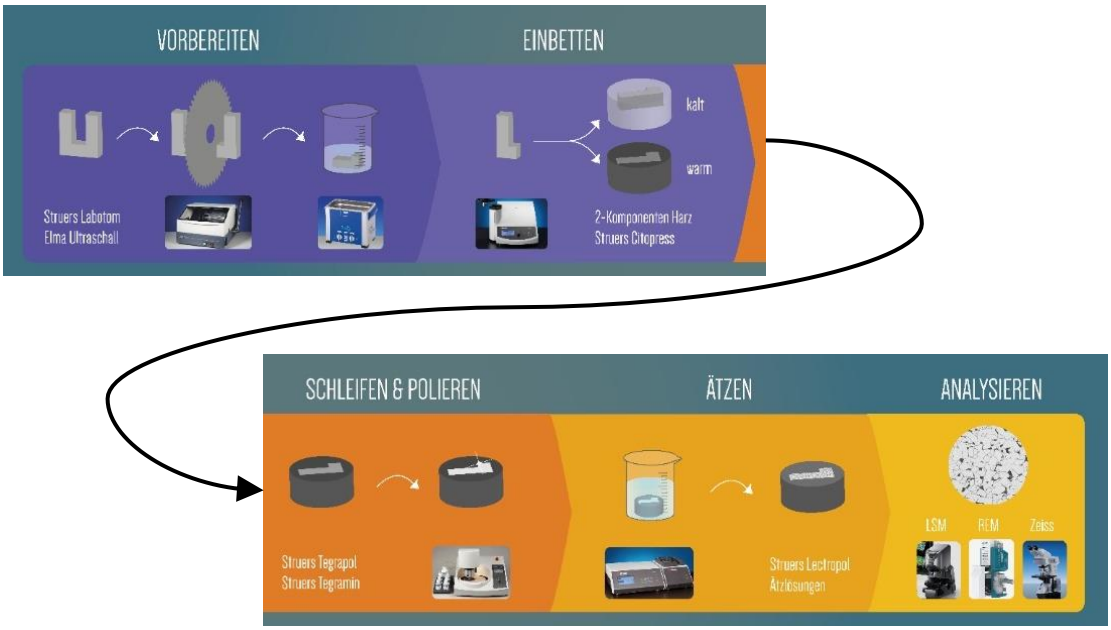

Fig. 5: Illustration of the different steps of the metallography process. Titles in German (left to right, top to bottom) read: "preparation", "embedding", "sanding & polishing", "etching" and "analysis". Bottom row specifies devices and materials used. Adapted from: Prof. Arne Wahlen, Fachhochschule Nordwestschweiz.

Surface composition

The composition of the griddle's original surface (before sanding) was determined through EDS (Energy-Dispersive X-ray Spectroscopy), using a scanning electron microscope (Zeiss Supra 40VP). The sections were chosen based on topographically interesting elements, namely grape-like structures (spectrum 25), a crater (spectrum 26) and a plane (spectrum 27), as seen on Fig. 14.

EDS works by shooting electrons at the sample. These electrons may knock an electron belonging to a lower shell of a sample's atom out, causing an electron from an energetically higher shell to fall into its old place. The energy difference is then released as a photon with an energy belonging to the X-ray spectrum [33]. Since every element possesses orbitals with energetic levels exclusive to itself, also the X-rays that are emitted belong to one element. So, by measuring the energy of the X-ray, the composition of the sample can be determined.

Surface imaging

The original surface of the griddle was imaged using a scanning electron microscope (Zeiss SUPRA 40VP). Scanning electrons microscopes (SEMs) work by shooting electrons (primary electrons) at a surface and detecting the ones that are reflected [33]. The volume in which the electrons interact with the sample is referred to as the electron-matter interaction volume. Specific signals can escape from certain depths of a volume [34]. Of those signals, there are two types of electrons important for imaging: Secondary electrons and back scattered electrons [33].

Secondary electrons are emitted from the section closer to the surface, through inelastic scattering, that is by an interaction which results in a transfer of energy from the primary electron to the electrons in the interaction volume [33], [35]. The primary electrons can knock electrons that are bound only lightly by the nucleus, such as valance electrons, out of their shell [35]. These secondary electrons are then detected, and an image is rendered [33].

Back-scattered electrons are emitted from the section of the interaction volume right below the secondary electrons [34]. They are the result of elastic interactions with the sample, that means no kinetic energy is lost by the primary electron through the interaction [36]. When approaching an atom of the sample, the primary electron is attracted by the nucleus, and reflected out of the sample. This is comparable to a gravity assist that a spaceship might use [37], [38]. Heavier elements tend to scatter the primary electrons more strongly than lighter elements. Because of that, the heavier elements will appear lighter on the image. Therefore, this type of detection provides insight into the composition of the sample [38].

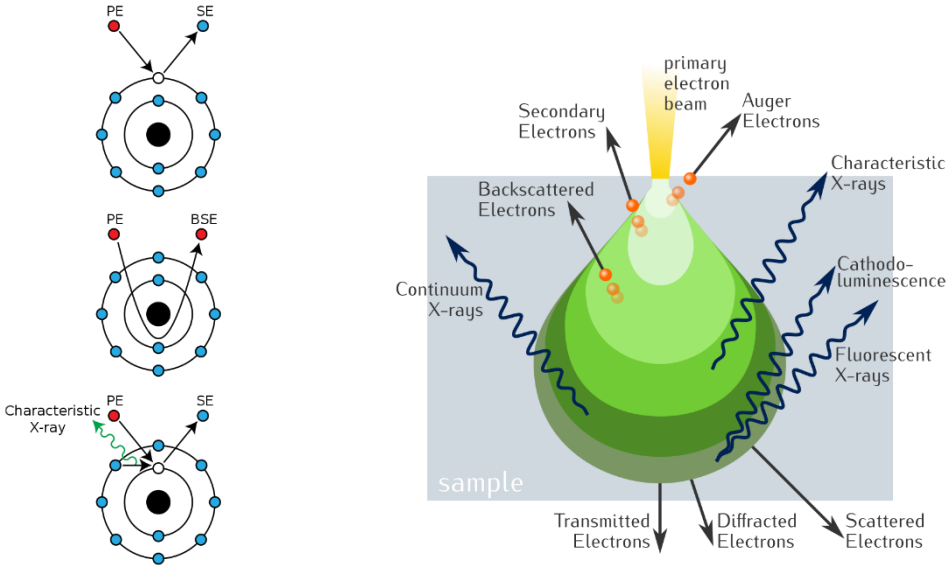

Fig. 6: Illustrations of the interactions of electrons resulting in the emission of different signals used in SEM imaging and EDS analysis (left), and the electron interaction volume, with the origin of the different signals highlighted (right). Drawings by Rob Hurt (left) and Ponor (right), both distributed under a Creative Commons Attribution-Share Alike 4.0 International license.

Measurement of Surface roughness

The surface roughness of the samples was determined using a laser scanning microscope (Keyence VK-X100 series). The surface roughness of samples 3, 7, C and D, along with a sample of the griddle's original surface, were measured. Samples 3, 7, C and D were imaged using 20x magnification, the sample with the original surface at 5x and 20x magnification. For the 20x magnification, the section was chosen to be of approximately 520 µm by 700 µm size. For the 5x magnification, the area was approximately 2050 µm by 2750 µm large. Two measurements were made, using 20x magnification for samples 3, 7, C and D: Sa (arithmetical mean height) and Sz (maximum height). A three-dimensional map of the surface section was rendered for all samples as well. The two metrics (Sa and Sz) describe the roughness of a surface. They are defined as follows:

The Sa describes the average of the absolute value of all peaks and valleys relative to the mean plane of the surface [39],

$$S_a = \frac{1}{A}\iint_A |z(x,y)|dxdy$$

Sz is calculated by summation of the absolute values of the size of the highest peak and the lowest valley within a given area [40].

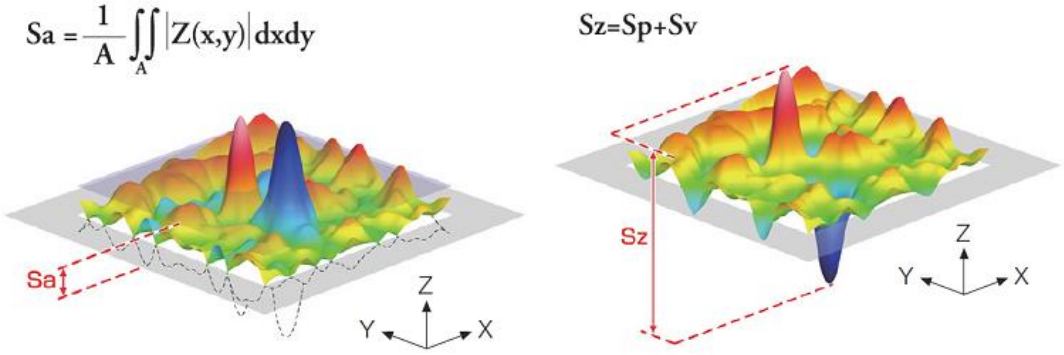

Fig. 4: Illustration of 3D-model of a surface, with roughness parameters Sa (left) and Sz (right) described. Images by Olympus Industrial Microscopes, sourced from [41].

Contact angle measurements

Contact angles were measured by two different methods: The first method used a Zeiss Axio Imager.M2 light microscope and a mirror rig (a mirror attached to a sample holder at a 45° angle). The sample was illuminated from the front using a LED panel, and the microscope's light source was turned off.

One drop of water was placed manually onto the surface using an Eppendorf pipette, with a drop volume of 2.5 µl. Once the drop was placed on the sample, a picture was taken, and the contact angle analysed by manually setting the tangent in the imaging software. The contact angles on both sides of the drop, CA(l) and CA(r), were measured.

In the second method, contact angle measurements were performed with a Krüss DSA 100 Drop Shape Analyzer. From every drop placed on the sample, two contact angles were measured, the one on the left (from the perspective of the camera), CA(l), and the one on the right, CA(r). The mean of both angles was calculated, CA(m). Per sample, between 3 and 7 drops were measured. The mean of the contact angle CA(m) of all drops in a sample and the standard deviation were calculated, resulting in one mean value for a sample. All contact angles provided in this paper were measured with the second method.

Results

CONTACT ANGLES

The contact angles were measured to determine the hydrophobicity of the samples. As described in the method, the contact angles were first measured using a Zeiss Axio Imager.M2 light microscope and a mirror rig. Yet, this method proved to be unreliable. Therefore, the contact angles of all samples were measured using a Krüss DSA 100 Drop Shape Analyzer. All contact angles published in this paper were determined using the second method.

Statistical analyses were performed to determine whether there was a significant difference between the means of certain batches of samples. To do that, first a one-way analysis of variance (ANOVA) was performed, followed by a multiple comparisons test (Tukey-Kramer test). The confidence interval was set to 95 %, therefore P-values ≤ 0.05 were considered to represent statistically significant differences.

Effect of Number of Heating Cycles

To determine whether and how the number of heating cycles influences the contact angle, samples undergoing one to five cycles were compared. All samples were coated with 1 mg/cm² of lamb tallow. Table 5 lists the measured contact angles for those samples, plus for Controls B (no tallow application, heated for 5 cycles) and C (sanded surface, but otherwise left untreated).

Increasing the number of cycles appeared to have a beneficial effect on the hydrophobicity, as evidenced by an increase in the measured contact angle from a single cycle to three heating cycles (Fig. 7). More cycles did not further increase the contact angle, but, in fact, tended to reduce it. Interestingly and unexpectedly, the completely untreated control sample (no surface coating, no heat cycling) featured similar hydrophobicity as those with multiple heat treatments. Also rather intriguingly, the control sample with heat treatment (5 cycles) but no surface treatment had substantially worse hydrophobicity than all other samples.

Table 5

		Cycles						
		1	2	3	4	5	B	C
	Drop							
CA(m) [°]	1	86.21	79.55	111.9	100.63	98.46	51.72	95.17
	2	76	92.29	113.06	87.24	91.49	54.23	90.96
	3	83.32	87.96	104.69	93.37	102.78	54.51	75.57
	4	75.43	99.15	100.57	92.62	91.31	-	-
	5	75.82	106.36	97.39	102.74	92.78	-	-
	6	89.85	95.34	108.55	101.08	-	-	-
	7	92.17	91.2	91.02	-	-	-	-
Mean CA(m) [°]		82.68	93.12	103.88	96.28	95.36	53.49	87.23

Contact angle as a function of the number of incubation cycles. CA(m) measurements for different drops on samples using ~1 mg/cm² lamb tallow, and 450°C goal temperature. 'Cycles' indicates number of cycles the sample underwent (not the sample number). Controls B and C are control samples. No tallow was applied to B, and it underwent 5 cycles. Control C was untreated.

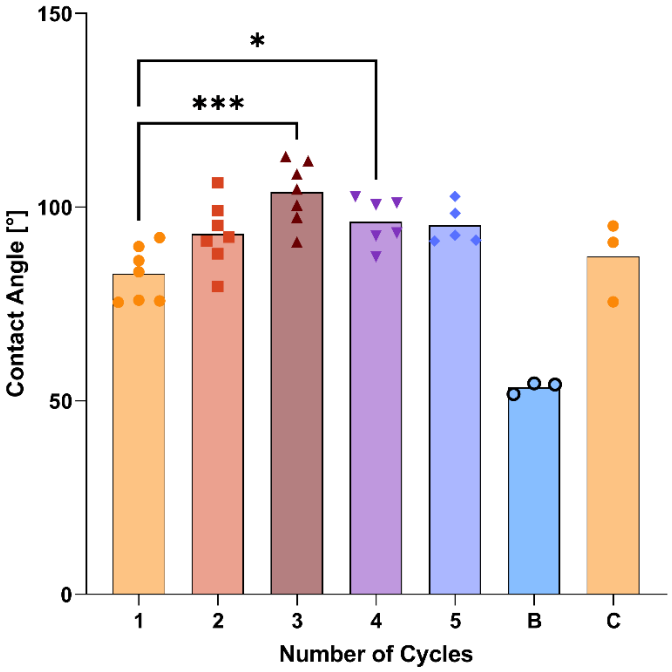

Fig. 7: Contact angles of samples undergoing a different number of cycles at 450°C, using ~1 mg/cm² of lamb tallow. Scatter corresponds to CA(m) measurements, bars illustrate the mean of the points. Brackets show significant differences between samples. One asterisk corresponds to a p value ≤ 0.05, two correspond to p ≤ 0.01, three to p ≤ 0.001 and four to p ≤ 0.0001. Significant differences with respect to controls are not shown to avoid overloading the figure, but they exist between Control B and every other sample, including C (all ****), and between C and 3 (*).

Effect of Amount of Lamb Tallow

To determine whether and how the amount of lamb tallow influences the contact angle, samples with different amounts of lamb tallow (ca. 1 mg/cm², 1.5 mg/cm², 2.5 mg/cm², 3 mg/cm²) were heated at 450°C for 5 cycles and were compared. Table 6 lists the measured contact angles for those samples, plus for Controls B (no tallow application, heated for 5 cycles) and C (left untreated).

Increasing the amount of tallow appeared to have a negative effect on the hydrophobicity, as evidenced by a decrease in the measured contact angle when going from 20 mg to 60 mg (Fig. 8). Increasing the tallow to 80 mg decreased the contact angle further; however, the difference was not statistically significant. Control C exhibited higher hydrophobicity than all samples except the one that was coated with 20 mg of tallow. Between those two, the difference was not statistically significant. Control B exhibited the third highest contact angle of all, although the difference between it and 40 mg was statistically insignificant.

Table 6

		Amount of lamb tallow [mg]					
		20	40	60	80	B	C
	Drop						
CA(m) [°]	1	98.46	59.92	36.12	32.8	51.72	95.17
	2	91.49	52.42	32.94	35.86	54.23	90.96
	3	102.78	47.92	42.58	31.31	54.51	75.57
	4	91.31	52.14	42.86	34.9	-	-
	5	92.78	50.77	42.12	19.76	-	-
	6	-	49.61	37.4	33.66	-	-
	7	-	44.74	42.22	30.85	-	-
Mean CA(m) [°]		95.36	51.07	39.46	31.3	53.49	87.23

Contact angle as a function of the amount of lamb tallow applied to the sample plate. CA(m) measurements for multiple drops on samples that underwent 5 cycles at 450°C. 'Amount of lamb tallow' refers to the absolute amount of tallow used for the samples (25 cm^2). Controls B and C are control samples. No tallow was applied to B, and it underwent 5 cycles. Control C was untreated.

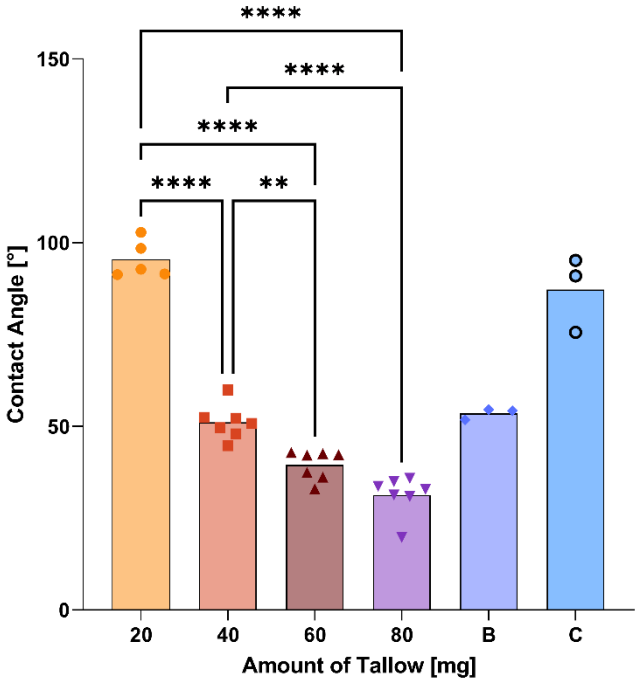

Fig. 8: Contact angles of samples using different amounts of lamb tallow at 5 cycles, 450°C. Scatter corresponds to CA(m) measurements, bars illustrate the mean of the points. Brackets show significant differences between samples. For explanation of asterisks, see caption Fig. 7. Significant differences with respect to controls (not shown) are between: Controls B and C, B and 20, B and 80 (all ****), B and 60 (**), and C and 40, C and 60, C and 80 (all ****).

Effect of Amount of Beef Tallow

To determine whether and how the amount of beef tallow influences the contact angle, samples with different amounts of beef tallow (ca. 1 mg/cm^2, 2.5 mg/cm^2, 3 mg/cm^2) were heated at 450°C for 5 cycles and were compared. Table 7 lists the measured contact angles for those samples, plus for controls B (no tallow application, heated for 5 cycles) and C (left untreated).

Increasing the amount of tallow appears to have a beneficial effect on the hydrophobicity, as evidenced by an increase in the measured contact angle from 20 mg to 60 mg of beef tallow (Fig. 9). More tallow did not further increase the contact angle,

but, in fact, tended to reduce it. Once again, the completely untreated control C (no surface coating, no heat cycling) featured similar hydrophobicity as those with surface coating. Control B exhibited again the lowest contact angles of all samples and controls.

Table 7

		Amount of beef tallow [mg]				
		20	60	80	B	C
CA(m) [°]	Drop					
	1	76.92	102.09	84.23	51.72	95.17
	2	72.15	95.71	84.82	54.23	90.96
	3	78.93	105.73	91.04	54.51	75.57
	4	95.53	110.4	95.02	-	-
	5	77.9	110.8	97.64	-	-
	6	81.09	103.06	94.85	-	-
	7	91.42	108.47	87.87	-	-
Mean CA(m) [°]		81.99	105.18	90.78	53.49	87.23

Contact angle as a function of the amount of beef tallow applied to the sample plate. CA(m) measurements for multiple drops on samples that underwent 5 cycles at 450°C. 'Amount of beef tallow' refers to the absolute amount of tallow used for the sample. Controls B and C are control samples. No tallow was applied to B, and it underwent 5 cycles. Control C was untreated.

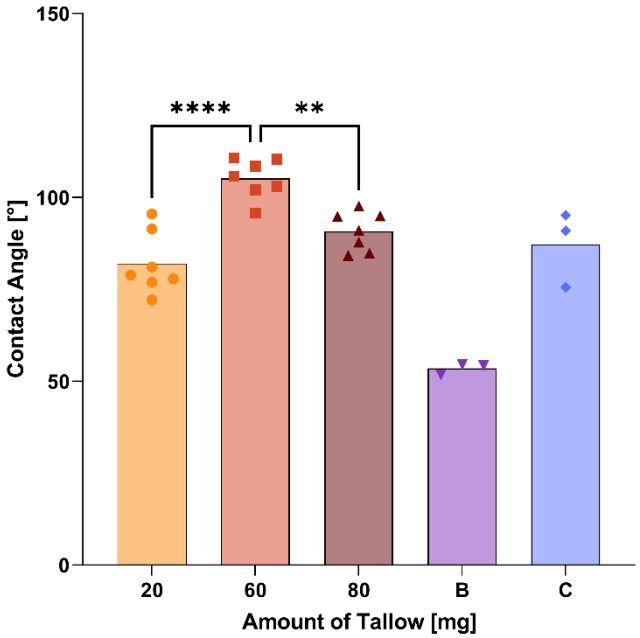

Fig. 9: Contact angles of samples using different amounts of beef tallow at 5 cycles, 450°C. Scatter corresponds to CA(m) measurements, bars illustrate the mean of the points. Brackets show significant differences between samples. For explanation of asterisks, see caption Fig. 7. Significant differences with respect to controls (not shown) are between: Control B and each other sample, including C (all ****), and C and 60 (**).

Effect of Different Reagents

To determine whether and how different reagents influence the contact angle, samples heated at 450°C for 5 cycles were compared. They were each coated with ca. 3 mg/cm² of a different reagent. Table 8 lists the measured contact angles for those samples, plus for controls B (no tallow application, heated for 5 cycles) and C (left untreated).

The beef tallow sample exhibited the highest hydrophobicity, followed by oleic acid, myristic acid and palmitic acid, although the differences between those three samples were not statistically significant (Fig. 10). The stearic acid and lamb tallow samples exhibited the worst contact angles. Between those two, the difference was also not statistically significant. Surprisingly, the completely untreated control C (no surface coating, no heat cycling) exhibited the second largest contact angle. This time, the contact angle of control B was average when compared to the other samples.

Table 8

		Reagents							
		LT	BT	MR	OL	ST	PL	B	C
	Drop								
CA(m) [°]	1	32.8	84.23	65.62	61.7	41.6	43.5	51.72	95.17
	2	35.86	84.82	47.82	54.32	38.84	30.69	54.23	90.96
	3	31.31	91.04	49.54	59.33	49.72	54.24	54.51	75.57
	4	34.9	95.02	-	-	-	60.56	-	-
	5	19.76	97.64	-	-	-	41.78	-	-
	6	33.66	94.85	-	-	-	-	-	-
	7	30.85	87.87	-	-	-	-	-	-
Mean CA(m) [°]		31.3	90.78	54.33	58.45	43.39	46.15	53.49	87.23

Contact angle as a function of the type of reagent applied to the sample plate. CA(m) measurements for multiple drops on samples that underwent 5 cycles at 450°C. Approximately 3 mg reagent per cm^2 was used. LT: lamb tallow, BT: beef tallow, MR: myristic acid, OL: oleic acid, ST: stearic acid, PL: palmitic acid. Controls B and C are control samples. No reagent was applied to B, and it underwent 5 cycles. Control C was untreated.

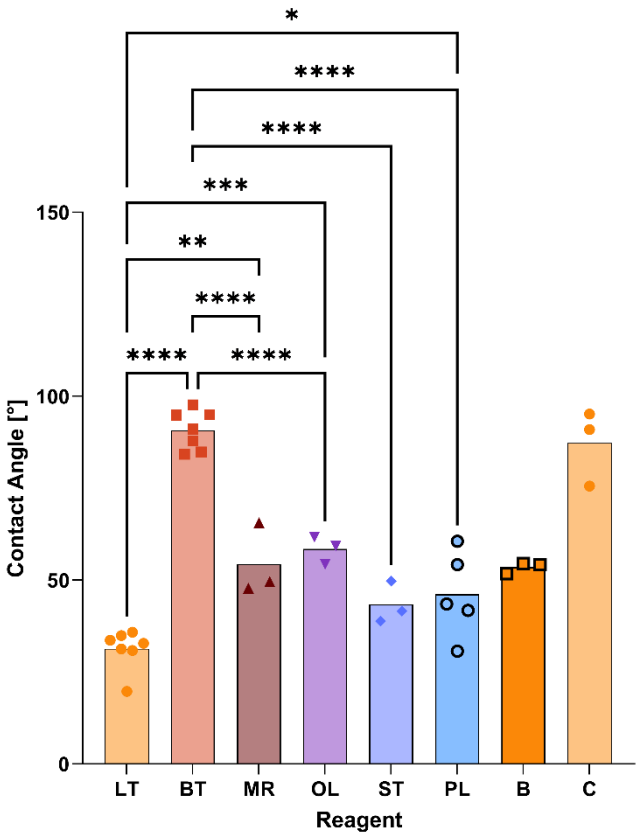

Fig. 10: Contact angles of samples using ~3 mg/cm^2 of different reagents at 5 cycles, 450°C. LT: lamb tallow, BT: beef tallow, MR: myristic acid, OL: oleic acid, ST: stearic acid, PL: palmitic acid. Scatter corresponds to CA(m) measurements, bars illustrate the mean of the points. Brackets show significant differences between samples. For explanation of asterisks, see caption Fig. 7. Significant differences with respect to controls (not shown) are between: Controls B and C (***), B and LT (**), B and BT(****), C and LT (****), C and MR (***), C and OL(**), C and ST(****), C and PL (****).

POSSIBLE RUST FORMATION

At some point during their treatment, orange residue exhibiting a similar appearance to rust was found on samples that underwent surface treatment with tallow. This residue appeared to be attracted by magnets. No residue was found on Sample B, which only underwent heat treatment. No measurements could be made to support that this residue was rust, or that would allow interpretation of the residue occurrence (see discussion section)

SURFACE IMAGING

The surface of the griddle was imaged using an SEM (Zeiss Supra 40VP) to gain insight into its topography. Similar structures to those analysed in the EDS analysis (Fig 14) were chosen to be examined.

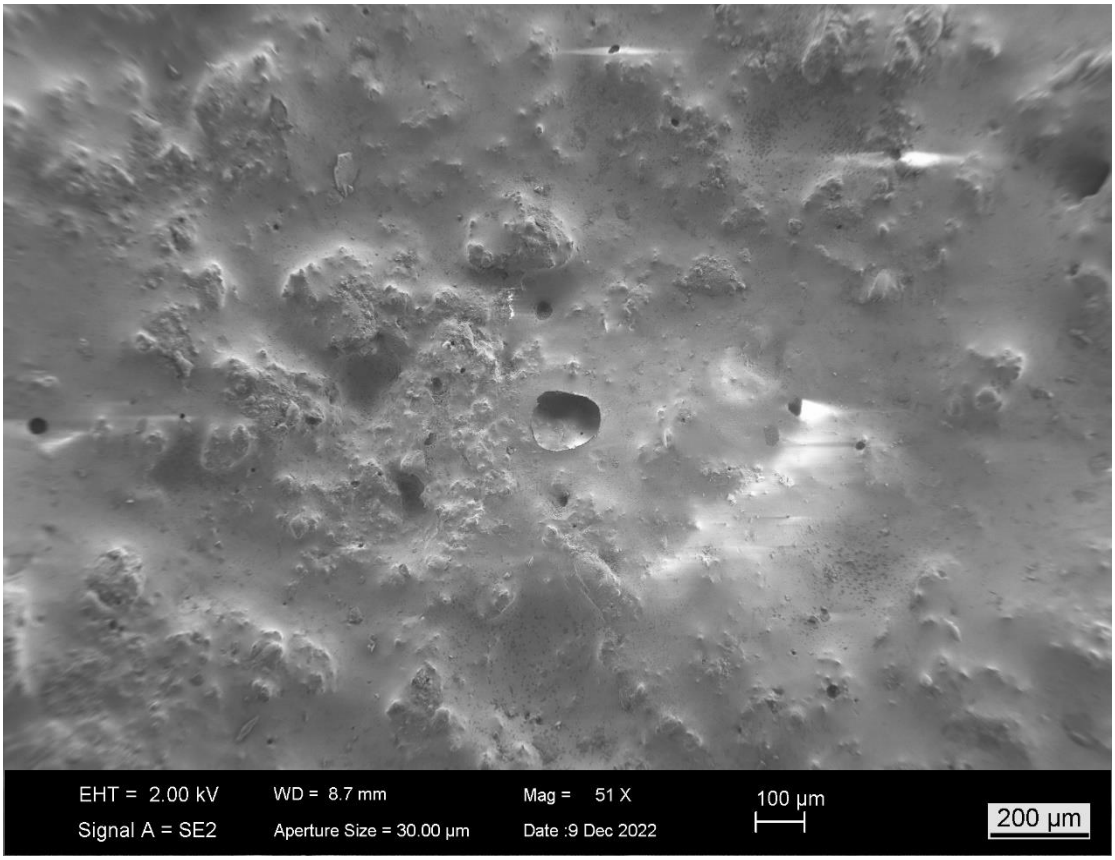

Fig. 11: SEM image of griddle surface, taken by a Zeiss Supra 40VP. This section was chosen to further examine craters and planes on the sample. The centre of the image shows a crater, which is magnified in Fig. 12.

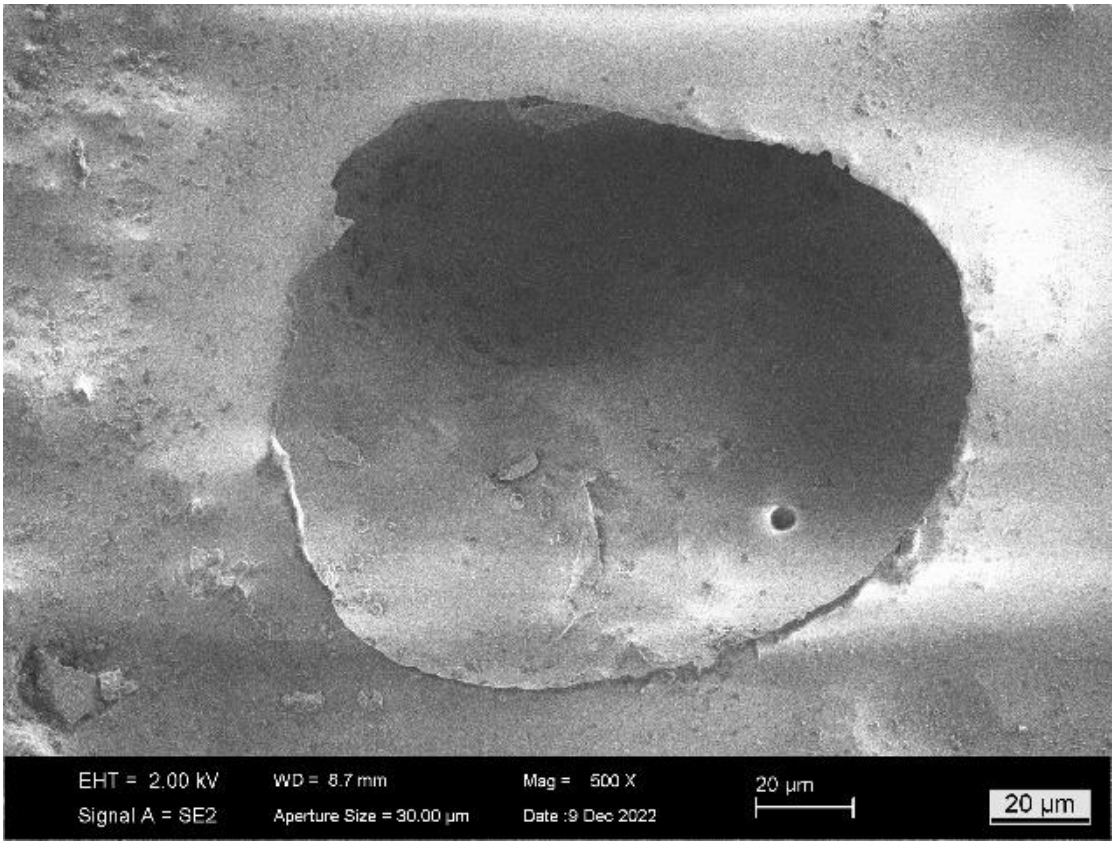

Fig. 12: Magnification of center crater in Fig. 11.

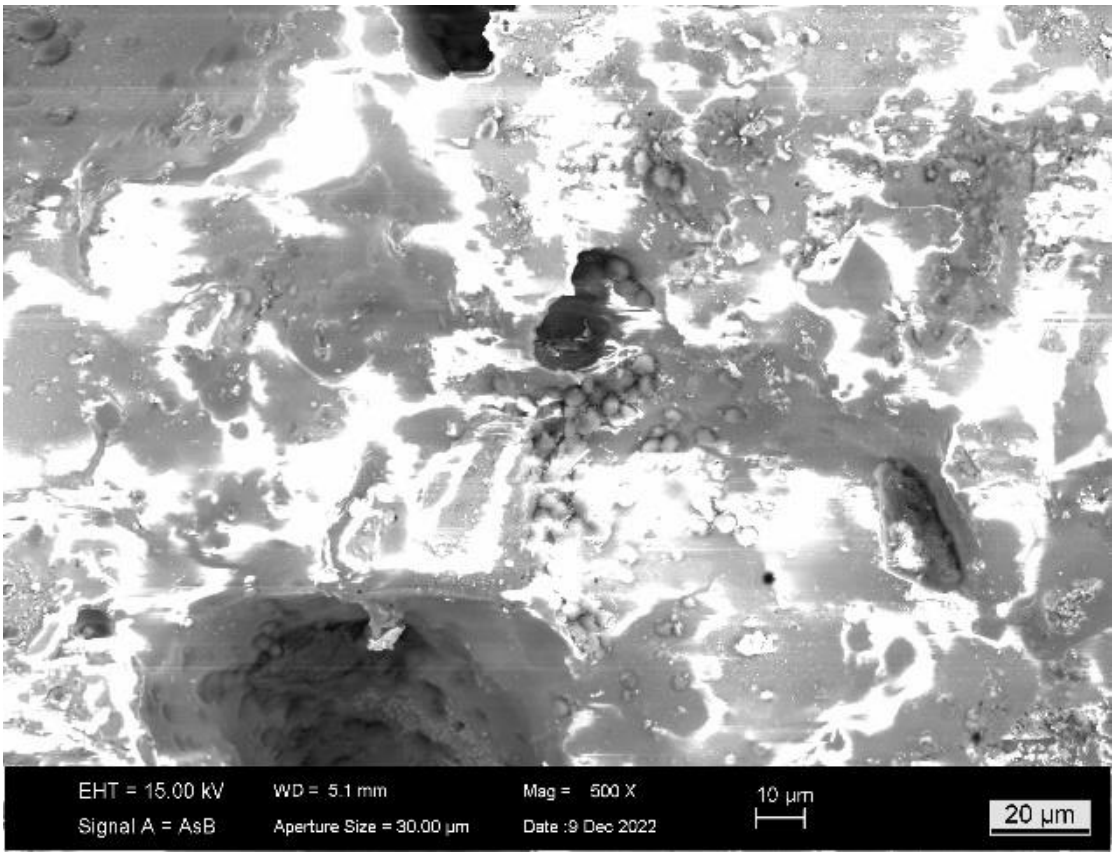

Fig. 13: SEM image of the grape structures described in the method section, taken with a Zeiss Supra 40VP.

SURFACE COMPOSITION

To gain more information on the surface composition of the griddles original surface, an EDS analysis of three different sections on the samples surface (Fig. 14) was performed using a Zeiss Supra 40VP scanning electron microscope. The sections were chosen based on topographically interesting elements, namely grape-like structures (Spectrum 25), a crater (Spectrum 26) and a plane (Spectrum 27). The results are summarized in Table 9.

Table 9

		Spectrum			
		25	26	27	Mean
	Element				
Weight percentage	C	46.2	65.95	10.91	41.02
	O	28.57	27.23	52.08	35.96
	Na	4.37	1.06	9.75	5.06
	Mg	0.66	0.24	2.15	1.02
	Al	2.41	0.1	4.68	2.4
	Si	8.01	0.23	13.01	7.08
	P	0.2	0.05	-	0.12
	S	0.27	0.47	0.07	0.27
	Cl	-	0.88	-	0.88
	K	1.27	1.00	1.49	1.25
	Ca	4.18	0.8	2.75	2.58
	Ti	-	-	0.67	0.67
	Mn	0.27	-	0.23	0.25
	Fe	0.14	0.27	0.28	0.23
	Cu	-	0.34	-	0.34
	Ba	2.11	-	1.73	1.92
	Pb	1.33	1.37	0.21	0.97

Surface composition of the griddle's original surface at defined locations (Fig. 14), determined through EDS analysis using a Zeiss Supra 40VP scanning electron microscope. Numbers are in weight percent. Columns are per location (label: spectrum) at which the EDS analysis was performed, plus mean (last column). Rows are per chemical element. Where no percentage is listed, the respective element's concentration in the sample section was under the detection limit.

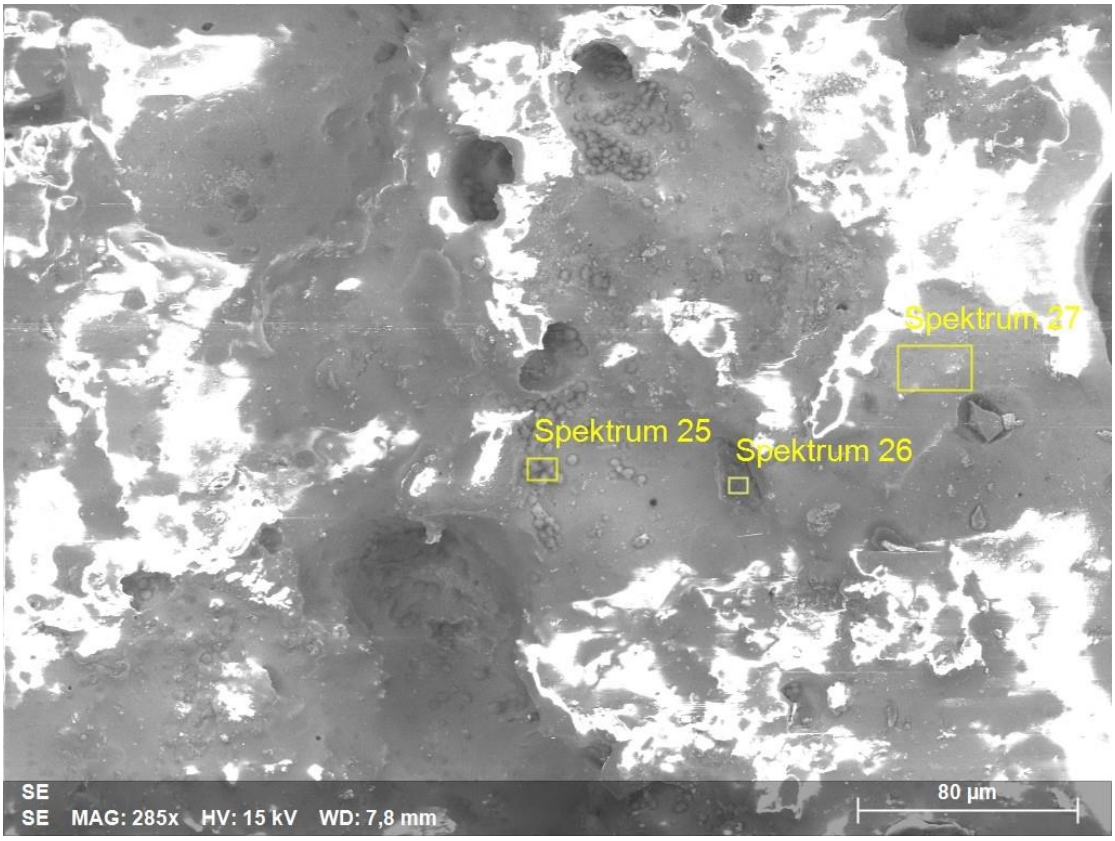

Fig. 14: SEM image (Zeiss Supra 40VP) of locations on griddle sample used to determine its composition.

SURFACE ROUGHNESS

Surface roughness was determined to properly characterize the topography of the samples. A laser scanning microscope (Keyence VK-X100 series) was used to measure the surface roughness by quantifying Sa and Sz (Table 10), and to render a three-dimensional map of the sample's surface (Figs. 20-23). The surface roughness of the different samples is extremely variable, especially surprising is the large difference in roughness between Samples D and C, since both were left untreated.

Table 10

Sample	Sa [µm]	Sz [µm]
3	1.374	13.548
7	0.889	20.204
C	0.806	11.714
D	1.483	16.404

Sa and Sz values of samples 3, 7, D and C

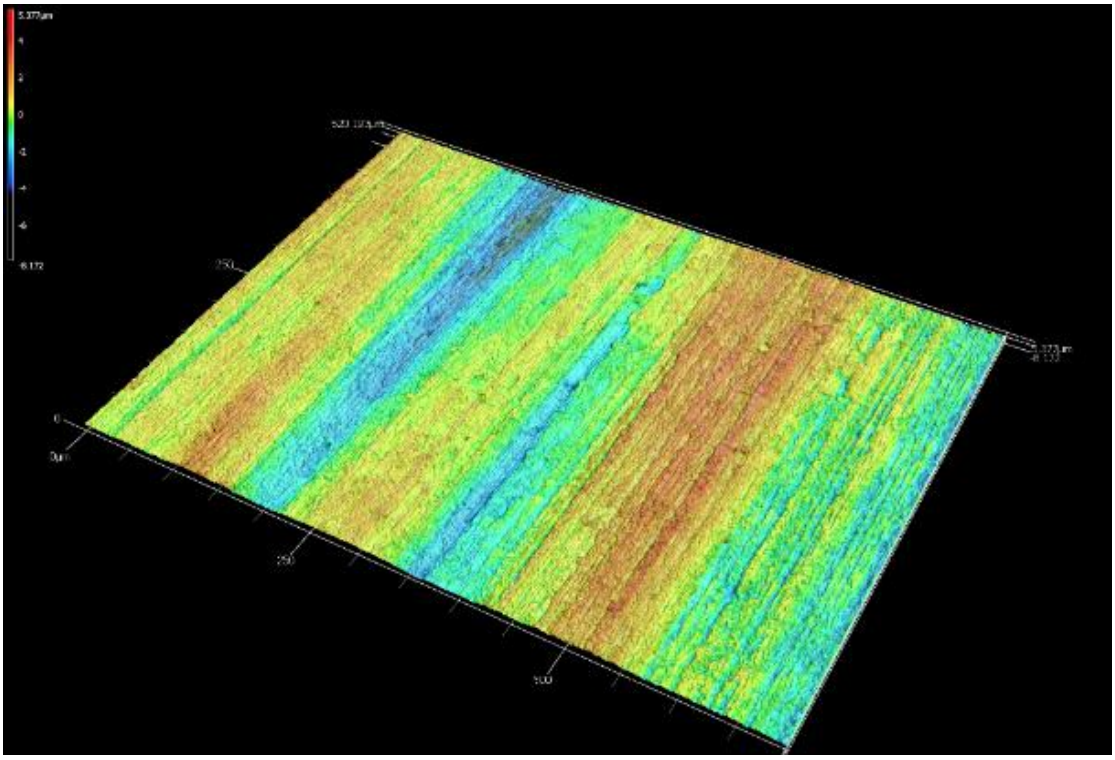

Fig. 20: 3D-map of Sample 3 produced using a Keyence VK-X100 series laser scanning microscope at 20x magnification.

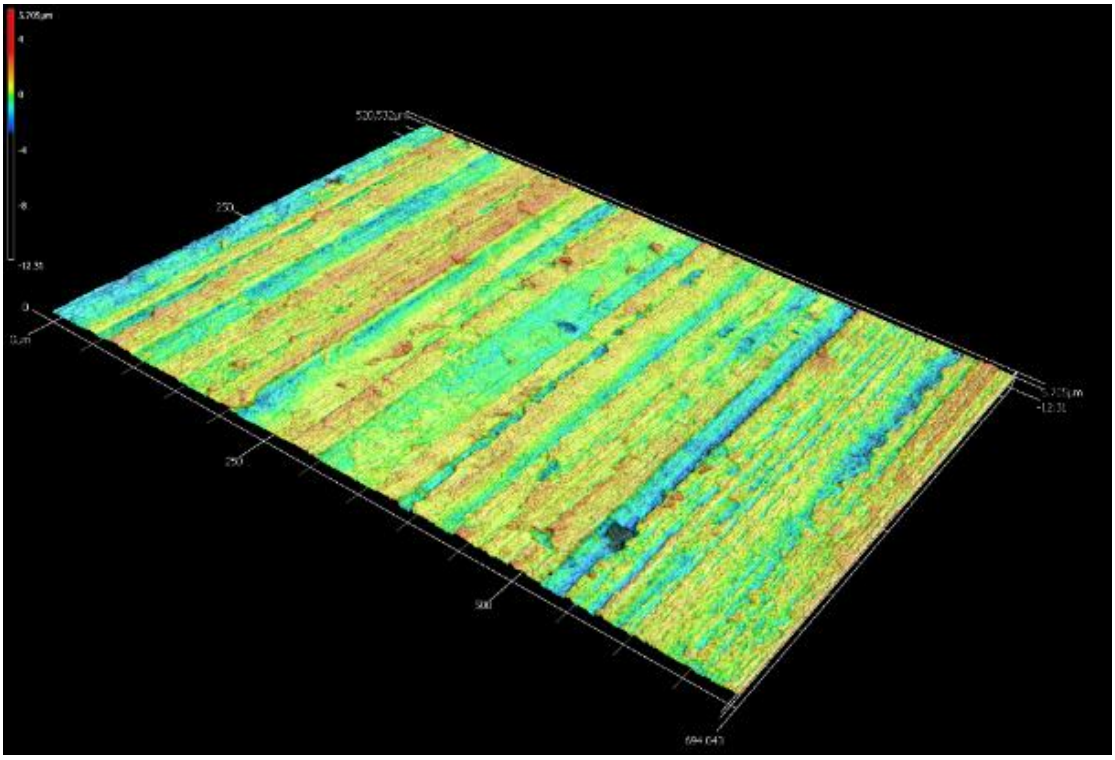

Fig. 21: 3D-map of Sample 7 produced using a Keyence VK-X100 series laser scanning microscope at 20x magnification.

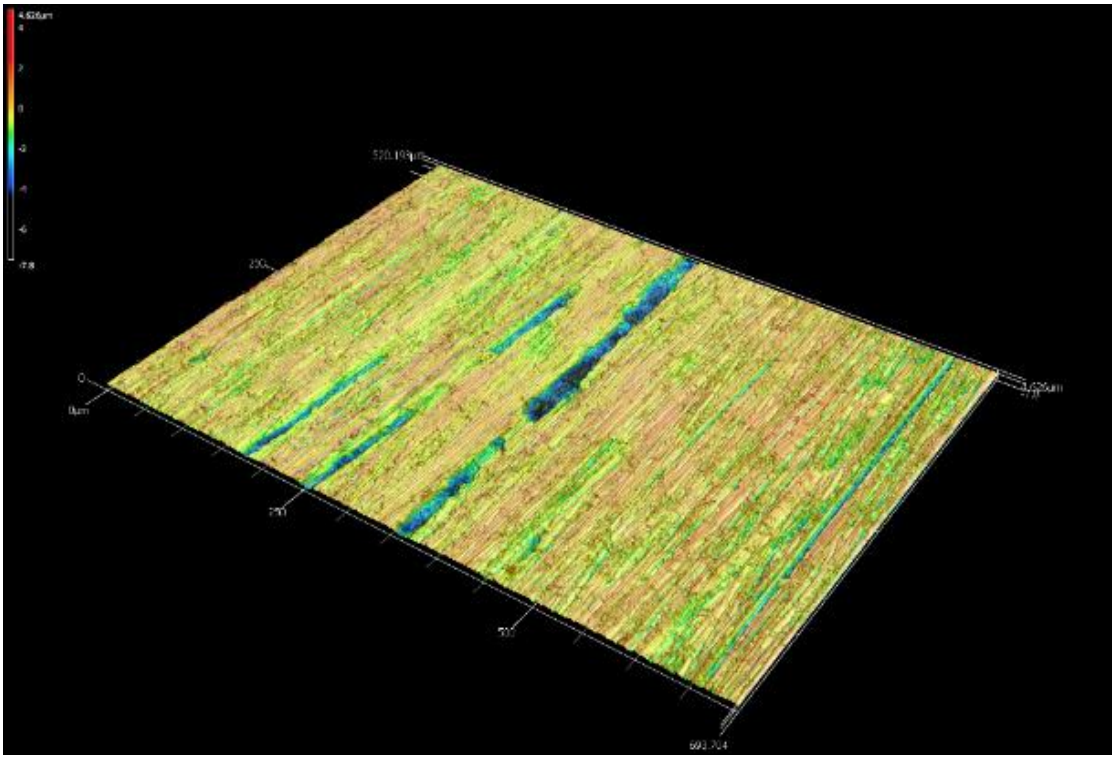

Fig. 22: 3D-map of Control C produced using a Keyence VK-X100 series laser scanning microscope at 20x magnification.

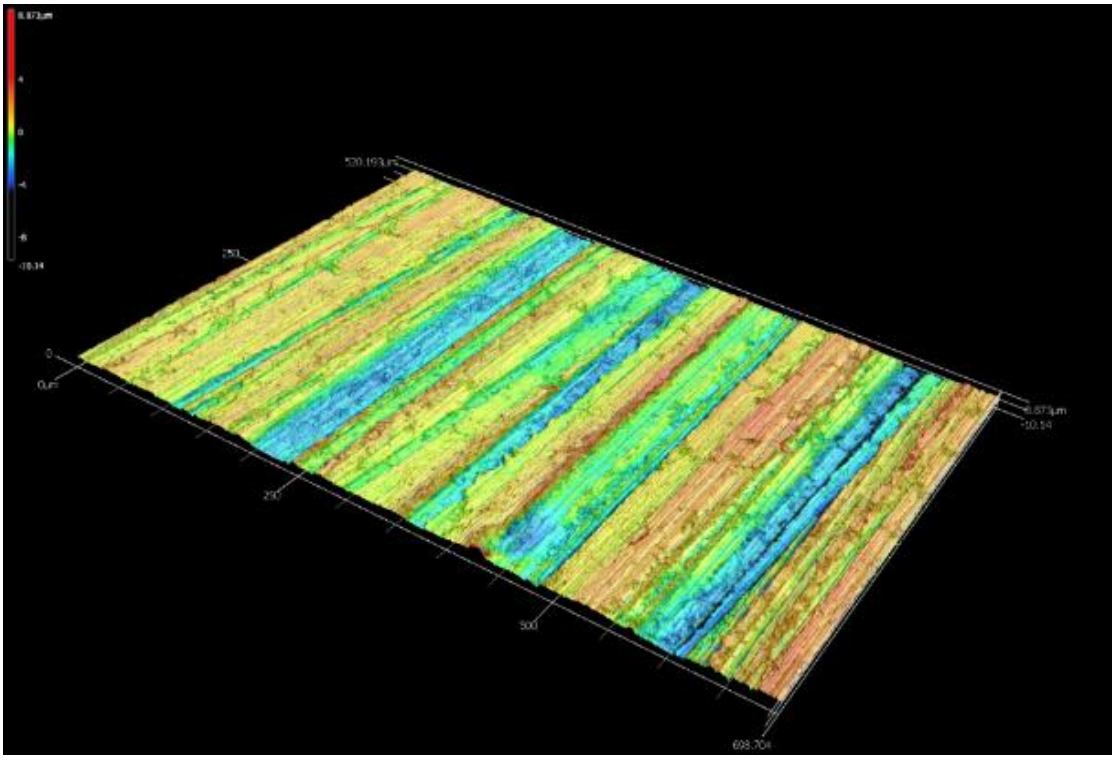

Fig. 23: 3D-map of control D produced using a Keyence VK-X100 series laser scanning microscope at 20x magnification.

ANALYSIS OF MATERIALS

Two samples underwent metallography to analyse the structure of the cast iron that was used. Images of both samples at 200x, 500x and 1000x magnification were taken (Fig. 18). As shown in Fig. 16, different structures are visible, including graphite, ferrite, and pearlite.

Graphite is a form of elemental carbon. It is built up out of many layers of carbon, arranged in a hexagonal grid (Fig. 17). A single layer is called graphene [42], [43]. Ferrite, also known as α-iron, is an allotrope of iron[44]. Allotropes of an element are different structural versions of itself [45]. For example, graphite and diamond are allotropes of carbon. Iron allotropes exhibit different crystal structures, as seen in Fig. 15 [46]. Pearlite is a material composed of cementite lamellae (Fe_3C) embedded in a ferrite matrix [47] (Fig. 19). Additionally, dot structures can be seen to aggregate around the lamellae. These structures are also composed of cementite. The orange coloration is a result of an interference pattern, which comes into play when the distance between the pearlite lamellae is smaller than the wavelength of the light [47].

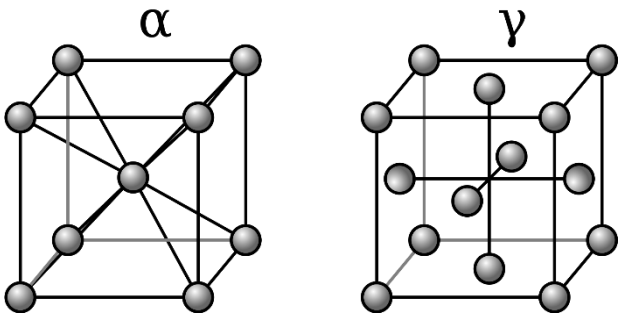

Fig. 15: Crystal structure of α- and γ-iron illustrated by unit cells. Illustration by Cdang, distributed under a Creative Commons Attribution-Share Alike 3.0 Unported license.

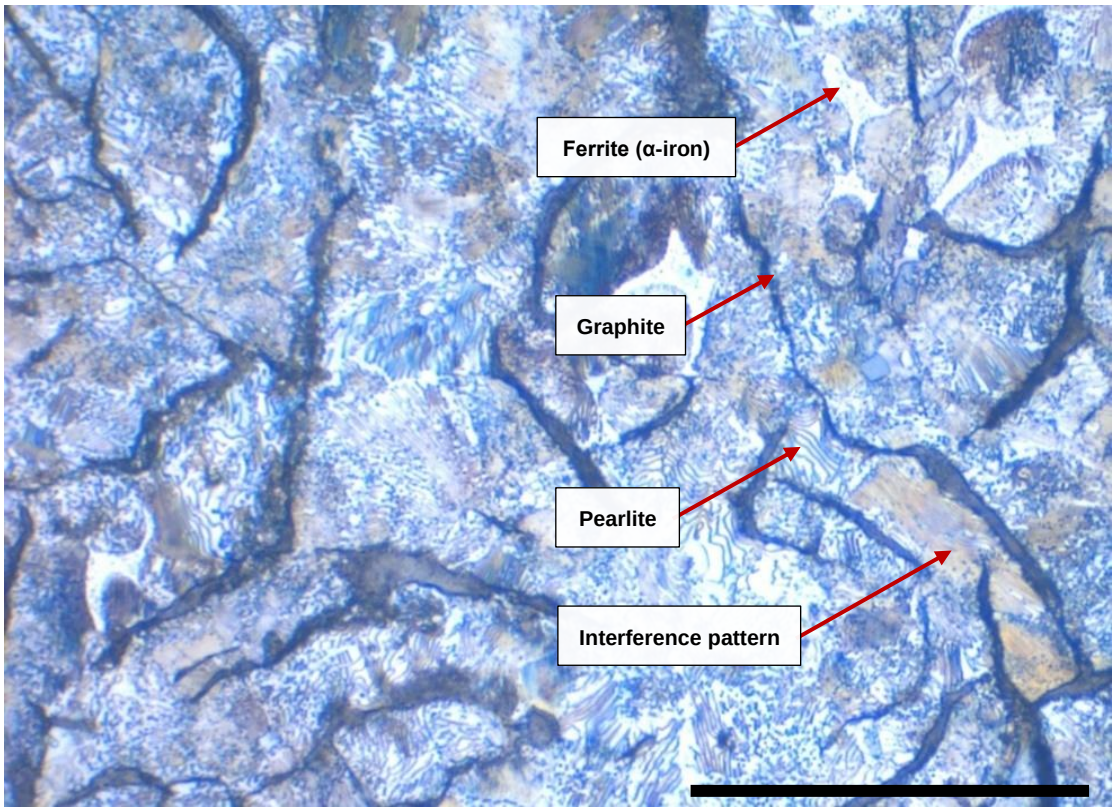

Fig. 16: Structures and composition of cast iron (griddle sample), adapted from Prof. Arne Wahlen. Scale bar: 50 µm.

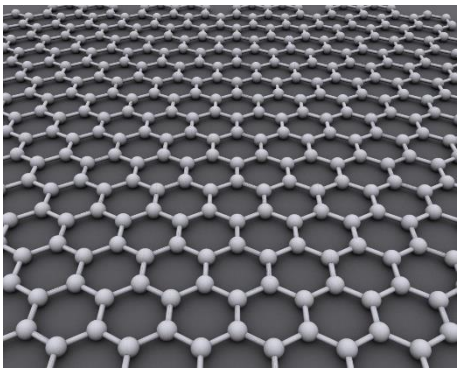

Fig. 17: Trigonal-planar arrangement of carbon atoms in graphene. The resulting hexagonal grid is nicely visible. Illustration byAlexanderAIUS, distributed under a Creative Commons Attribution-Share Alike 3.0 Unported license.

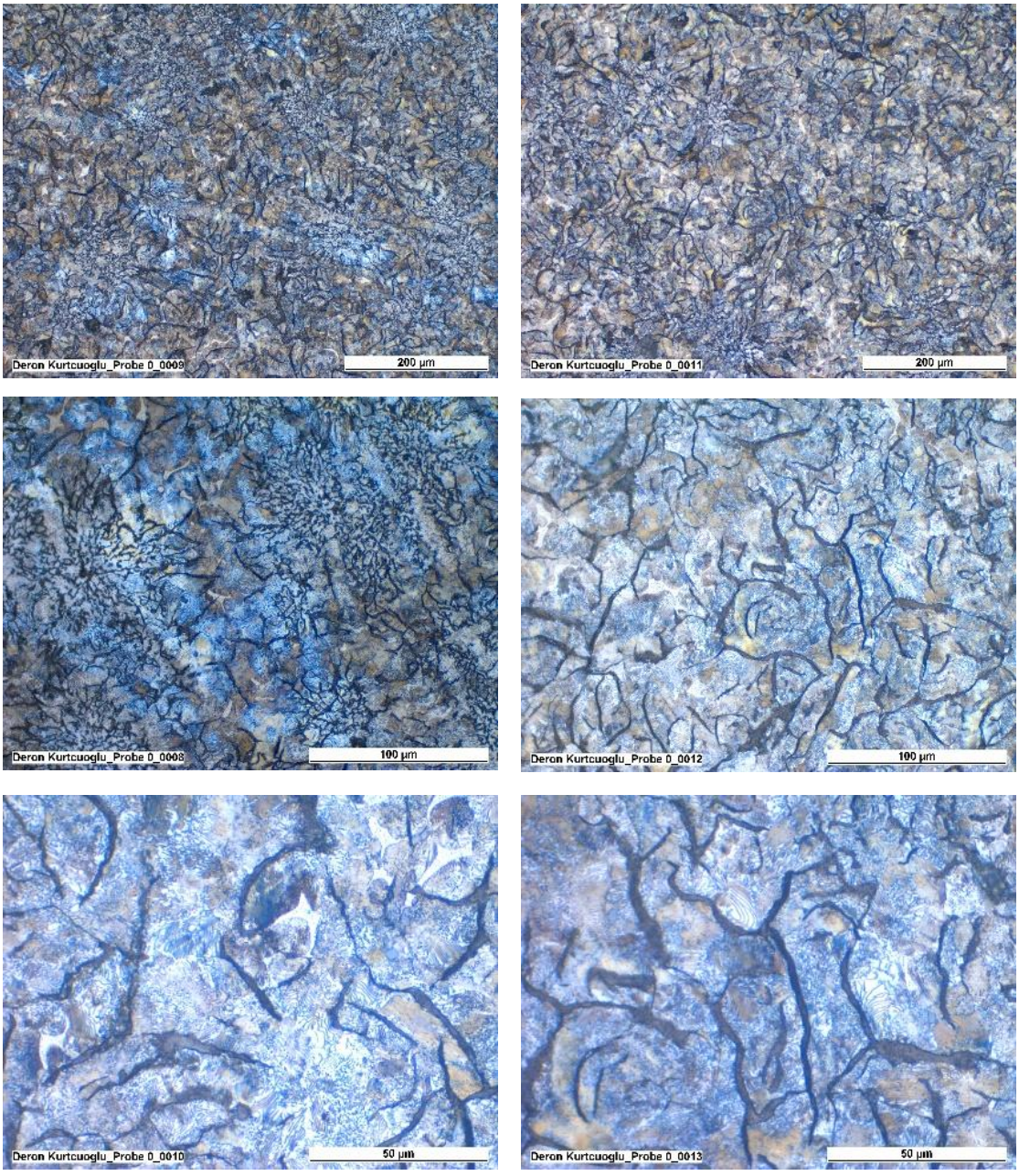

Fig. 18: Comparison of samples griddle (left) and B (right) at 200x, 500x and 1000x magnification.

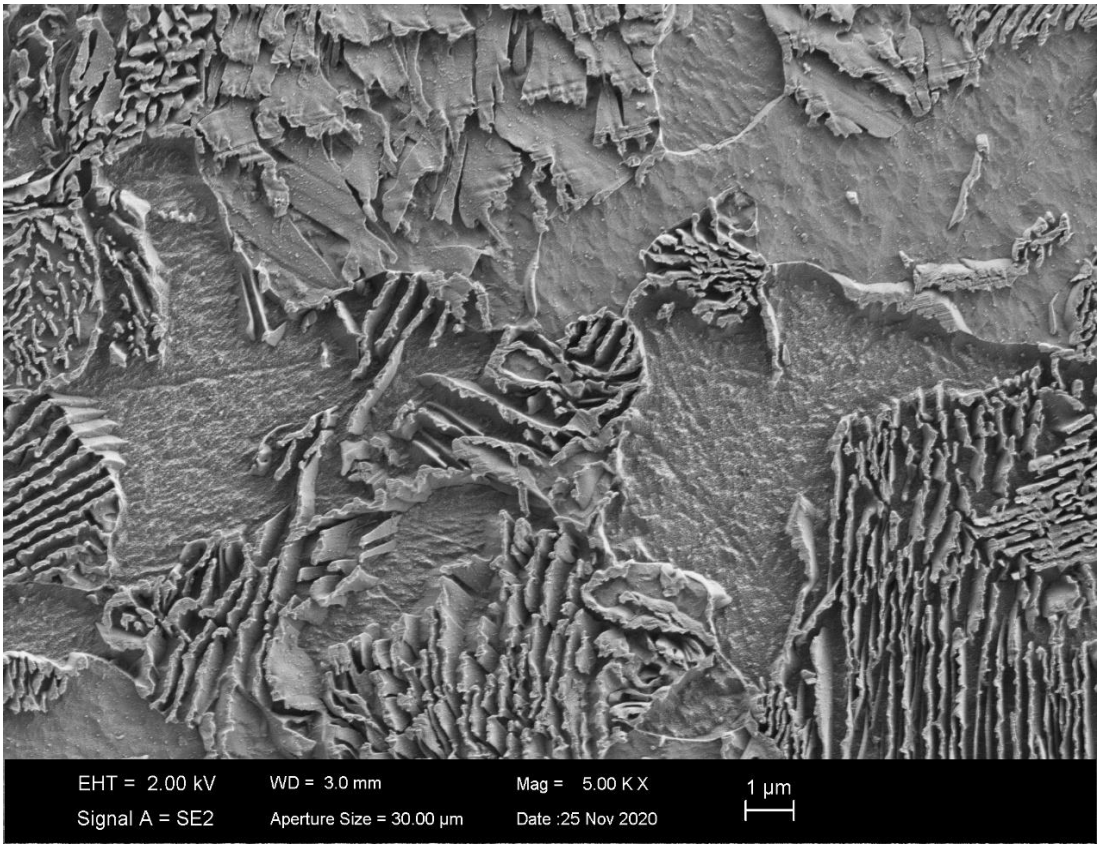

Fig. 19: Pearlite under SEM. Provided by Prof. Arne Wahlen, Fachhochschule Nordwestschweiz.

Discussion and Outlook

Starting with the premise that the seasoning-process of cast-iron pans increases their hydrophobicity, multiple experimental series were conducted to determine how the implementation of different factors affect the contact angle of water on the surface. The primary aim of this study was to investigate the effects of such parameters on the seasoning of cast-iron pans, such as the number of treatment cycles, the type, and the amount of reagent. To this end, samples were prepared by varying the chosen parameters and the contact angle, surface roughness and surface composition of the samples were measured.

When looking at the effect of the number of cycles on the hydrophobicity of the sample, it became clear that an increase from one to three cycles led to larger contact angle. Increasing the number of cycles further did not increase the contact angle, but in fact tended to decrease it, although the difference between cycles 3, 4 and 5 were not statistically significant. This was surprising, since in the paper from which the reference process was taken records the sample that underwent 5 cycles as having the highest contact angle [17]. This may be attributed to various factors, linked both to the preparation of the samples and the measurement of the contact angle.

On the preparation side, subsequent communication with the authors of that research paper (Prof. Dr. Li Cunpu, School of Chemistry and Chemical Engineering, Chongqing University, PR China) revealed that the samples “should be annealed in the furnace to room temperature, to avoid the [cracking] of the formed iron-oxide layer” (this rather

than removing the sample directly after the incubation time and letting it cool at environmental temperature). Further, Prof. Li stated that the layer of tallow "should be a little bit thick, [because] we need the decomposition of the oil to form the carbon catalytic layer, then to induce the formation of the iron-oxide layer." Additionally, the tallow should "fully cover the surface of the plate. Therefore, the oxygen cannot diffuse to the iron surface until the fat decomposed." The latter aspect was accommodated by the experiments in this paper. Prof. Li also guesses that the layer should be thicker than 1 mm, although the relationship between the amount of fat and the iron morphology was not studied by him and his team. This discrepancy between their work and this paper may have arisen as a consequence of partially incomplete information available in their paper and its published supplemental data [17].

A further aspect on the preparation side is the amount of tallow used in the first experimental series. Although the average amount of tallow for Sample 1 (5 cycles) was equal to 22 mg, the amount of tallow used before each cycle varied between 8 and 38 mg. This could explain why the contact angle of Sample 1 did not reach the one described in the reference, as the formation of the nanoballs apparently relies on the increase of the oxygen partial pressure PO_2, which in turn is facilitated by the tallow evaporation. If, therefore, the amount of tallow is very small, and takes little time to evaporate, there might not be enough time for the change in iron atom coordination to take place to the degree necessary for the formation of the nanoballs. However, this is not backed up by the experiment with different amounts of lamb tallow, since the contact angle is continuously reduced with an increase of the amount of lamb tallow used. While this is true, it must be recalled that Sample 1 itself was used in the analysis of that experiment. Additionally, the average amount of tallow of Samples 1-5 varied within a range of 9 mg, from 19 to 28 mg. For the aforementioned reasons, this difference could be interpreted as an explanation why Sample 3 exhibited the largest contact angle, but once again further experiments conducted in this paper contrast this hypothesis. The reason for this unequal use of the amount of tallow can be traced back to uncertainty on how to best prepare the samples at the start of the experiments, and failure to recognize the extent of the flaw upon further examination, which could have prevented this deficiency.

Another limitation on the preparation side was the original surface roughness. When first roughness measurements were performed, the sample exhibiting the highest contact angle (Sample 3) was compared to a sample with very low contact angles (Sample 7) and Control C (untreated). The difference in surface roughness became increasingly interesting when the roughness of a second untreated control was measured (Control D). The striking difference in between the two controls means that the different samples are very likely to have had different surface conditions in the first place, making it even harder to quantify the effect of the chosen parameters on the resulting hydrophobicity. Ideally, the surface roughness of all samples would have been measured, which would have answered this question, but due to time constraints this was not possible.

On the measurement side, too few measurements were made to make a meaningful statement on the contact angle and whether the difference between the hydrophobicity of the different samples was statistically significant, especially regarding the controls and the samples using myristic, oleic and stearic acid, where only three measurements each were made.

The tendency of the contact angle to decrease in the experiment examining the effect of the amount of lamb tallow was unexpected to begin with. However, the measurement of the samples that were prepared to study the effect of the amount of beef tallow made it altogether more intriguing: When the amount of beef tallow was increased from 20 to 60 mg, the contact angle increased. While further increasing the amount did not further increase the contact angle, but rather decreased it, this is in contrast with the lamb tallow experiment. It would be intriguing to attribute the described behaviour to the type of tallow used, but the limitations of the experiments do not allow for this interpretation. Once again, these limitations can be attributed to factors linked to the preparation of the samples and their measurement:

On the preparation side, although the mean amounts of tallow used for Samples 6-11 were all within ± 3 mg of the target, the amount of tallow used before each cycle varied strongly (amounts for Sample 6 were within a range of 11 mg, Sample 7 within a range of 9 mg, Sample 8 within a range of 7 mg, Sample 9 within 5 mg, Sample 10 within 19 mg, and Sample 11 within 15 mg). This makes it hard to determine the effect of a given amount of tallow on the contact angle, as the actual amount used did not always correspond to the amount of tallow that was supposed to be used during the experiment. Further limitations that can be attributed to the preparation include the cooling method and the surface roughness, as discussed earlier.

The experiment series comparing the use of different reagents also showed somewhat surprising results. Firstly, regarding the fatty acid samples. one might assume that the sample with the reagent that evaporates the slowest would show the highest contact angle, since that sample should facilitate high oxygen partial pressure the longest. This appears not to be the case, however, as stearic acid has the lowest contact angle and the highest boiling temperature of the group. The boiling temperatures are as follows: MR, 326°C; PL, 352°C; OL, 360°C; ST, 371°C [48]–[50]. Intriguingly, oleic acid, the only reagent in the group that is a liquid at room temperature, has the second highest boiling point. Originally, the low melting point had been interpreted as meaning that it would evaporate the fastest. Furthermore, of all the fatty acids, the sample coated with oleic acid exhibited the largest contact angles, although no difference within Samples 18-21 was statistically significant. The contrast between the results and the hypothesis mentioned at the beginning of this paragraph can be due to various factors, again linked to the preparation and measurement, but also linked to the hypothesis:

On the hypothesis side, perhaps the whole concept of contact angles increasing with longer evaporation times is not appropriate. This would be strongly supported by the experiment with the amount of lamb tallow, and partially by the beef tallow equivalent, when looking at the difference between the 60 and 80 mg sample. However, the limitations of these experiments discussed earlier once again do not allow for this conclusion to be drawn. These limitations also effect the results obtained during the different reagent experiment, further increasing the difficulty of interpreting the results.

The orange residue occurrence was surprising, since Gao et al. only described rusting at 600°C [17]. Unfortunately, determining whether the residue was in fact rust through Prussian Blue synthesis [51], [52] was unsuccessful, due to poor extraction methods for the residue, and limited amount of extracted material. Because of this, interpretation of the occurrence of the residue could not be made.

Regarding the materials chosen, the cross-sectional analysis of the cast iron led to the discovery of dot-structured cementite. This structure is formed during the heat

treatment of cast-iron from the lamellae, due to its lower surface area being more thermodynamically favourable [47]. This lets us draw the conclusion that the griddle itself was heat treated during production, since this structure was found not only in Control B, which was heat-treated for this paper, but also in the untreated griddle sample. Furthermore, the surface composition analysis interestingly suggested the presence of lead (Pb). This leads to the question of whether this poses a health risk, and if so, how one can avoid the purchase of contaminated cookware.

For further studies of the contact angle of seasoned cast-iron, the following should be taken into account: Firstly, the statistical analysis must be considered already during the experiment design, and by extension the sample size and number of measurements as well. Additionally, the size of the samples should be uniform, to where an equal number of measurements can be taken. Secondly, the surface roughness of all samples must be provided for, since this led to uncertainty during this study. While it was a limiting factor, it could be used as a further parameter in future experiments. Thirdly, after each cycle a sample undergoes, contact angle measurements should be made, to collect more precise data on the development thereof. Furthermore, surface imaging should be used to control the initial surface parameters of the samples at the beginning of the experiment and whenever possible after a treatment cycle. Unfortunately, this was not possible during this study, due to the risk of fat residue damaging the SEM. For future studies, either a way to image the surface under the SEM without risk of damage to both the SEM and the sample (due to cleaning methods), or a different approach must be chosen altogether. Moreover, a better way to apply the reagent, both for the tallow and fatty acids, must be found. One of the biggest limitations, the inconsistency of the amount of reagent used, can be attributed to a poor application approach. Additionally, the uniformity of the reagent coating must be accounted for. Furthermore, the samples must be annealed in the furnace, as described by Prof. Li Cunpu. Moreover, more controls must be used, and for controls such as B, that only underwent heat treatment, contact angles should be measured after each cycle. And finally, the occurrence of the orange residue must be researched, and in case of it being rust, further research should go into the prevention of its formation.

Although many limitations plagued the study, it was certainly not unsuccessful. The insight gained on how to proceed with the experiments alone is sufficient to call this study a success. Furthermore, over a third of the samples (1, 2, 3, 4, 7 and 8) out of 15 total exhibited a larger contact angle than both Controls B and C, and two of those samples exhibited statistically significant differences compared to Control C. Therefore, the goal of producing hydrophobic seasonings on cast-iron was indeed reached.

Summary

The goal of this paper was to gain insight into hydrophobic properties provided to cast-iron by the process of seasoning. To this end, the effects of the type and amount of reagent used for seasoning and the number of treatment cycles used was investigated, using the contact angle of a drop of water on the samples to quantify hydrophobicity. By doing so, the hope was to provide groundwork for the improvement of the classical non-stick coating of cast-iron pans and to supply a better alternative to PTFE cookware, whose production and consumption bring up a variety of pollution and sustainability concerns. By conducting experiments that compared variations of the chosen parameters, samples with a contact angle higher than the controls were successfully produced. Unfortunately, limitations that may be attributed to various factors, including limited sample size and initial surface conditions, did not allow to establish firm correlations between investigated parameters and hydrophobicity. However, because of some of these limitations, insight into how to proceed with new experiments and further ideas for parameters to study in the process of improving cast-iron seasoning were produced.

References

[1] Rebecca Rupp, "A Brief History of Cooking With Fire," Sep. 02, 2015. https://www.nationalgeographic.com/culture/article/a-brief-history-of-cooking-with-fire (accessed Dec. 28, 2022).

[2] X. Wu *et al.*, "Early Pottery at 20,000 Years Ago in Xianrendong Cave, China," *Science*, vol. 336, no. 6089, pp. 1696–1700, Jun. 2012, doi: 10.1126/science.1218643.

[3] W. Rosen, "The most powerful idea in the world: a story of steam, industry, and invention," in *The most powerful idea in the world: a story of steam, industry, and invention*, University of Chicago Press edition., Chicago: University of Chicago Press, 2012.

[4] Bennet Woodcroft, *Reference index of patents of invention, from 1617 to 1852, by B. Woodcroft*, vol. 1. Great Seal Patent Office, Southhampton Buildings, Holborn, 1855. Accessed: Dec. 29, 2022. [Online]. Available: https://archive.org/details/referenceindexpoooffigoog/page/n58/mode/2up

[5] H. McGee, *On Food and Cooking: the Science and Lore of the Kitchen*. New York: Scribner, 2007.

[6] P. Thomas, "The use of fluoropolymers for non-stick cooking utensils," *Surface Coatings International*, vol. 81, no. 12, pp. 604–609, Dec. 1998, doi: 10.1007/BF02693055.

[7] W. Nicole, "PFOA and Cancer in a Highly Exposed Community: New Findings from the C8 Science Panel," *Environmental Health Perspectives*, vol. 121, no. 11–12, Nov. 2013, doi: 10.1289/ehp.121-A340.

[8] EFSA Panel on Contaminants in the Food Chain (CONTAM) *et al.*, "Risk to human health related to the presence of perfluorooctane sulfonic acid and perfluorooctanoic acid in food," *EFS2*, vol. 16, no. 12, Dec. 2018, doi: 10.2903/j.efsa.2018.5194.

[9] A. C. Ford, P. Moayyedi, and S. B. Hanauer, "Ulcerative colitis," *BMJ*, vol. 346, no. feb05 2, pp. f432–f432, Feb. 2013, doi: 10.1136/bmj.f432.

[10] S. Martinez-Hervas and J. F. Ascaso, "Hypercholesterolemia," in *Encyclopedia of Endocrine Diseases*, Elsevier, 2019, pp. 320–326. doi: 10.1016/B978-0-12-801238-3.65340-0.

[11] D. Trudel, L. Horowitz, M. Wormuth, M. Scheringer, I. T. Cousins, and K. Hungerbühler, "Estimating Consumer Exposure to PFOS and PFOA: Estimating Consumer Exposure to PFOS and PFOA," *Risk Analysis*, vol. 28, no. 2, pp. 251–269, Apr. 2008, doi: 10.1111/j.1539-6924.2008.01017.x.

[12] M. Sajid and M. Ilyas, "PTFE-coated non-stick cookware and toxicity concerns: a perspective," *Environ Sci Pollut Res*, vol. 24, no. 30, pp. 23436–23440, Oct. 2017, doi: 10.1007/s11356-017-0095-y.

[13] EPA, "Our Current Understanding of the Human Health and Environmental Risks of PFAS." https://www.epa.gov/pfas/our-current-understanding-human-health-and-environmental-risks-pfas (accessed Jan. 07, 2023).

[14] J. M. Caverly Rae, L. Craig, T. W. Slone, S. R. Frame, L. W. Buxton, and G. L. Kennedy, "Evaluation of chronic toxicity and carcinogenicity of ammonium

2,3,3,3-tetrafluoro-2-(heptafluoropropoxy)-propanoate in Sprague–Dawley rats," *Toxicology Reports*, vol. 2, pp. 939–949, 2015, doi: 10.1016/j.toxrep.2015.06.001.

[15] Chemours, "What is HFPO-Dimer Acid?" https://www.chemours.com/en/about-chemours/genx (accessed Jan. 08, 2023).

[16] Lesley Stockton, "The best Nonstick pan," *Wirecutter (NYT)*, Nov. 18, 2022. https://www.nytimes.com/wirecutter/reviews/best-nonstick-pan/#types-of-nonstick-coatings (accessed Dec. 26, 2022).

[17] C. Gao *et al.*, "Seasoning Chinese cooking pans: The nanoscience behind the Kitchen God's blessing," *Nano Materials Science*, p. S2589965120300416, Jun. 2020, doi: 10.1016/j.nanoms.2020.06.001.

[18] Wikipedia, "Hydrophobe." https://en.wikipedia.org/wiki/Hydrophobe (accessed Oct. 24, 2022).

[19] Steve Severtson, "Lecture Series 'Introduction to Surface and Colloid Science, Lecture 13: Contact Angle, Young's Equation and Wetting.'" Accessed: Jul. 30, 2022. [Online]. Available: https://www.youtube.com/watch?v=RrsF4iFUJ3M

[20] W. M. Sigmund and S.-H. Hsu, "Cassie–Baxter Model," in *Encyclopedia of Membranes*, E. Drioli and L. Giorno, Eds. Berlin, Heidelberg: Springer Berlin Heidelberg, 2016, pp. 310–311. doi: 10.1007/978-3-662-44324-8_1381.

[21] Y. Gu *et al.*, "Research progress of biomimetic superhydrophobic surface characteristics, fabrication, and application," *Advances in Mechanical Engineering*, vol. 9, no. 12, p. 168781401774685, Dec. 2017, doi: 10.1177/1687814017746859.

[22] W. M. Sigmund and S.-H. Hsu, "Wenzel Model," in *Encyclopedia of Membranes*, E. Drioli and L. Giorno, Eds. Berlin, Heidelberg: Springer Berlin Heidelberg, 2013, pp. 1–2. doi: 10.1007/978-3-642-40872-4_1380-2.

[23] Richard E. Dickenson and Irving Gates, "Bond Energy," in *Chemistry, Matter, and The Universe*, 3rd ed., W.A. Benjamin, INC., 1976, p. 13,46.

[24] Richard E. Dickenson and Irving Gates, "intramolecular forces," in *Chemistry, Matter, and The Universe*, 3rd ed., W.A. Benjamin, INC., 1976, p. 275.

[25] J. Zhang, "Surface Free Energy," in *Encyclopedia of Tribology*, Q. J. Wang and Y.-W. Chung, Eds. Boston, MA: Springer US, 2013, pp. 3443–3448. doi: 10.1007/978-0-387-92897-5_450.

[26] USGS, "Water in Space: How Does Water Behave in Outer Space?," *United States Geological Survey Website*. https://web.archive.org/web/20220517092337/https://www.usgs.gov/special-topics/water-science-school/science/water-space-how-does-water-behave-outer-space (accessed Jan. 08, 2023).

[27] Emma Spooner, "A Guide to Surface Energy." https://www.ossila.com/en-eu/pages/a-guide-to-surface-energy (accessed Jul. 30, 2022).

[28] A. J. Kinloch, "Surface energy values," in *Adhesion and Adhesives*, Dordrecht: Springer Netherlands, 1987, p. 26,30,33. doi: 10.1007/978-94-015-7764-9.

[29] H. Wang *et al.*, "Review: Porous Metal Filters and Membranes for Oil–Water Separation," *Nanoscale Res Lett*, vol. 13, no. 1, p. 284, Dec. 2018, doi: 10.1186/s11671-018-2693-0.

[30] C. W. Extrand and S. I. Moon, "Contact Angles on Spherical Surfaces," *Langmuir*, vol. 24, no. 17, pp. 9470–9473, Sep. 2008, doi: 10.1021/la801091n.

[31] Gonser, "Grillplatte Gusseisen 36.5 x 20 cm," *Gonser.ch*. https://www.gonser.ch/grillplatte-gusseisen-365-20-cm/a-18099/?ReferrerID=7& (accessed Jan. 08, 2023).

[32] Mahler und Co., "Brox Rindertalg zum Kochen," *Mahler und Co.* https://www.mahlerundco.ch/brox/3824-brox-bio-rindertalg-4260491771087.html?source=googleps&gclid=CjoKCQiAzeSdBhC4ARIsACj36uEfvTkFAX5rqN45CL1009tQ3z5TqiPgZz3ehFgz_ufXQNHT8BbiTroaAqWIEALw_wcB (accessed Jan. 08, 2023).

[33] R. Marassi and F. Nobili, "MEASUREMENT METHODS | Structural and Chemical Properties: Scanning Electron Microscopy," in *Encyclopedia of Electrochemical Power Sources*, Elsevier, 2009, pp. 758–768. doi: 10.1016/B978-044452745-5.00071-X.

[34] Antonis Nanakoudis, "SEM: Types of Electrons and the Information They Provide," Nov. 21, 2019. https://www.thermofisher.com/blog/materials/sem-signal-types-electrons-and-the-information-they-provide/ (accessed Jan. 08, 2023).

[35] J. I. Goldstein, D. E. Newbury, J. R. Michael, N. W. M. Ritchie, J. H. J. Scott, and D. C. Joy, "Secondary Electrons," in *Scanning Electron Microscopy and X-Ray Microanalysis*, New York, NY: Springer New York, 2018, pp. 29–37. doi: 10.1007/978-1-4939-6676-9_3.

[36] B. J. Inkson, "Scanning electron microscopy (SEM) and transmission electron microscopy (TEM) for materials characterization," in *Materials Characterization Using Nondestructive Evaluation (NDE) Methods*, Elsevier, 2016, pp. 17–43. doi: 10.1016/B978-0-08-100040-3.00002-X.

[37] Wikipedia, "Gravity assist." https://en.wikipedia.org/wiki/Gravity_assist (accessed Jan. 01, 2023).

[38] Erik Luyk, "Backscattered Electrons in SEM Imaging," Dec. 20, 2019. https://www.thermofisher.com/blog/materials/backscattered-electrons-in-sem-imaging/ (accessed Jan. 01, 2023).

[39] Keyence, "Sa." https://www.keyence.eu/ss/products/microscope/roughness/surface/parameters.jsp (accessed Dec. 31, 2022).

[40] Keyence, "Sz." https://www.keyence.eu/ss/products/microscope/roughness/surface/tab01_b.jsp (accessed Dec. 31, 2022).

[41] Olympus, "Surface Roughness Measurement—Parameters." https://www.olympus-ims.com/en/metrology/surface-roughness-measurement-portal/parameters/ (accessed Jan. 08, 2023).

[42] C. R. Holkar, S. S. Jain, A. J. Jadhav, and D. V. Pinjari, "Scale-Up Technologies for Advanced Nanomaterials for Green Energy," in *Nanomaterials for Green Energy*, Elsevier, 2018, pp. 433–455. doi: 10.1016/B978-0-12-813731-4.00014-X.

[43] Y. Meng, "Polymer/graphite nanocomposites," in *Polymer Nanocomposites*, Elsevier, 2006, pp. 510–539. doi: 10.1533/9781845691127.2.510.

[44] Wikipedia, “Allotropes of iron.” https://en.wikipedia.org/wiki/Allotropes_of_iron (accessed Jan. 02, 2023).

[45] V. Gold, Ed., *The IUPAC Compendium of Chemical Terminology: The Gold Book*, 4th ed. Research Triangle Park, NC: International Union of Pure and Applied Chemistry (IUPAC), 2019. doi: 10.1351/goldbook.

[46] N. G. Connelly, Royal Society of Chemistry (Great Britain), and International Union of Pure and Applied Chemistry, Eds., *Nomenclature of inorganic chemistry. IUPAC recommendations 2005*. Cambridge, UK: Royal Society of Chemistry Publishing/IUPAC, 2005.

[47] Arne Wahlen, “Direct Communication ‘Cast iron structure,’” Dec. 09, 2022.

[48] J. A. Young, “Chemical Laboratory Information Profile: Oleic Acid,” *J. Chem. Educ.*, vol. 79, no. 1, p. 24, Jan. 2002, doi: 10.1021/ed079p24.

[49] D. R. Lide and Chemical Rubber Company, Eds., *CRC handbook of chemistry and physics: a ready-reference book of chemical and physical data*, 90. ed., 2009–2010. Boca Raton, FLa.: CRC Press, 2009.

[50] IPCS, “Palmitic acid,” *INCHEM*. https://www.inchem.org/documents/icsc/icsc/eics0530.htm (accessed Jan. 06, 2023).

[51] LD DIDACTIC GMBH, “LD Handblätter Chemie, Allgemeine und Anorganische Chemie, Korrosionsschutz.” LD DIDACTIC GMBH. Accessed: Jan. 08, 2023. [Online]. Available: https://www.ld-didactic.de/documents/en-US/EXP/C/C1/C1534_d.pdf

[52] Truman State University, “Synthesis of Prussian Blue.” Truman State University. Accessed: Jan. 08, 2023. [Online]. Available: https://chemlab.truman.edu/files/2015/07/Synthesis-of-Prussian-Blue.pdf

Glossary

Allotrope	A distinct structural version of an element (e.g., diamond versus graphite as allotropes of carbon)
ANOVA	Statistical method to analyze differences between means of different groups
α-iron	See ferrite
BP	Before Present, timescale used in archeology, with January 1st, 1950, defined as start
Cast iron	Type of iron-carbon-alloy with carbon content >2%.
CA(l)	Contact angle measured at the left side of a drop (from the perspective of the microscope)
CA(m)	Mean of contact angles CA(l) and CA(r)
CA(r)	Contact angle measured at the right side of a drop (from the perspective of the microscope)
Coating	Thin layer of material on the surface of another material
Contact angle	Angle between a surface and a tangent to a droplet on the same surface at its three-phase line
DuPont	DuPont de Nemours, Incorporated. A multi-national chemical company headquartered in the USA. Producer of Teflon.
EDS	See energy-dispersive X-ray spectroscopy
Energy-dispersive X-ray spectroscopy	Method for measuring the elemental composition of a substance using X-rays
Fatty acid	Major building block of naturally occurring fats
Ferrite	Allotrope of iron with body-centered cubic crystal structure
Fe_3O_4	Iron(II,III) oxide, occurs naturally as magnetite
Graphite	Form of elemental carbon consisting of multiple layers arranged in a hexagonal grid
Griddle	Flat (with or without ridges) or convex cooking surface, often a flat metal plate

HFPO-DA	Chemical from the PFAS family, known commonly as GenX together with its ammonium salt.
Hydrophobicity	The ability of a substance to repel water. A hydrophobic surface is characterized by a water drop sitting on its surface having a contact angle ≥ 90°.
Hydrophilic	A hydrophobic surface is characterized by a water drop sitting on its surface having a contact angle < 90°.
Hypercholesterolemia	Levels of cholesterol in blood exceeding normal levels
Hypertension	High blood pressure
Incubation	Process of keeping an object at a specified elevated temperature
Interfacial tension	Mechanical force per area at the interface of two contacting substances with different state of matter
Interference pattern	Repeating bright and dark areas in an image produced by light interference
ISS	International Space Station
Laser scanning microscope	Light microscope that illuminates only small area of a sample with a laser before moving to the next, thereby increasing the obtainable resolution compared to traditional widefield microscopy
Metallography	Study of the microscopic structure of metal alloys
Monomer	Basic repeating unit of a polymer
Muffle furnace	Type of furnace in which the material being heated is in a compartment separated from that of the burning fuel
Myristic acid	Saturated fatty acid found, e.g., milk or coconut oil
Nital	Mixture of nitric acid and ethanol. Used to prepare metal samples for metallography.
Oleic acid	Mono-unsaturated fatty acid. In triglyceride form, it makes up large parts of various vegetable oils such as olive oil

Palmitic acid	Saturated fatty acid commonly found in animal fat
Pearlite	Ferrite matrix with inclusions of cementite lamellae
Per- and polyfluoroalkyl substances	Chemicals that possess a group consisting of at least two fluorine atoms bound to a carbon atom.
Perfluorooctanesulfonic acid	Surface-active substance (surfactant), colloquially referred to as a 'forever chemical' because of the amount of time it takes to decompose in nature.
Perfluorooctanoic acid	Surface-active substance (surfactant) from the family of per- and polyfluoroalkyls. Originally used to produce PTFE. Colloquially referred to as 'forever chemical'. Banned in Switzerland since 2021.
PFAS	See per- and polyfluoroalkyl substances
PFOA	See perfluorooctanoic acid
PFOS	See perfluorooctanesulfonic acid. Its use has been banned in some countries
Polymer	Molecule consisting of smaller repeating units
Polytetrafluoroethylene	Hydrophobic polymer built up out of C_2F_4 monomers, commonly known as Teflon
PO_2	Oxygen partial pressure
PTFE	See polytetrafluoroethylene
P-value	Statistical parameter that quantifies the likelihood that a difference between measured groups is due to chance rather than due to actual difference. A smaller P-value means smaller likelihood that the difference is coincidental.
Rendering	Process by which animal substances, such as animal fat, are converted into products with longer shelf life
Sa	Metric for surface roughness indicating arithmetic mean height of surface features
Scanning electron microscope	Apparatus for producing magnified images of the surface of a sample using focused electron beams

Seasoning	Procedure for coating pans and other cookware by heating of oil or fat on its cooking surface
SEM	See scanning electron microscope
Stearic acid	Saturated fatty acid found mostly in animal fat, but also in cocoa butter
Superhydrophobic	A superhydrophobic surface is characterized by a water drop sitting on its surface having a contact angle >150°.
Surface energy	Atomic bond energy surplus at the surface versus bulk of a material
Surface roughness	Variation in the height of a surface. Can be characterized with the metrics Sa and Sz.
Surface tension	Interfacial tension between a liquid and a gaseous substance in contact with each other
Sz	Metric for surface roughness indicating maximum peak to valley amplitude of surface features
Tallow	Rendered animal fat
Teflon	Brand name of a PTFE product produced by the company DuPont
Three-phase line	Boundary between a liquid drop, the surrounding gas, and the surface of the solid the drop sits on
Tukey-Kramer test	Statistical test to assess whether means of multiple groups are statistically different from each other
Ulcerative colitis	Medical condition characterized by long-term inflammation of parts of the gastrointestinal tract
Wetting condition	Complete wetting is characterized by zero contact angle, while partial wetting occurs with water on hydrophilic surfaces at contact angles above zero but below 90°.
XPS	See X-ray photoelectron spectroscopy
XRD	See X-ray diffraction analysis
X-ray diffraction analysis	Method for analyzing the crystal structure of a material using X-rays

X-ray photoelectron spectroscopy	Method for analyzing the chemical surface composition of a material using X-rays

Appendix

CONTACT ANGLE MEASUREMENTS

Sample 1

Table A1

Drop	CA(m) [°]	CA(l) [°]	CA(r) [°]	Volume [µL]	Temperature [°C]
1	98.46	99.46	97.46	3.052	22.3
2	91.49	91.47	91.51	3.188	22.5
3	102.78	102.48	103.07	3.213	22.6
4	91.31	91.79	90.84	3.289	22.7
5	92.78	93.69	91.88	2.394	22.7

Measurements of contact angles on Sample 1 for five different drops. CA(l), CA(r): contact angles on the left and right side of the drop, respectively, as seen in the microscope. CA(m): Mean of CA(l) and CA(r). The volume of the drops and the ambient air temperature at the time of the placement of the drop on the surface are also listed.

Table A2

Measured Entity	Mean	SD
CA(m) [°]	95.36	5.06
CA(l) [°]	95.78	4.93
CA(r) [°]	94.95	5.25
Temperature [°C]	22.6	0.2
Diameter [mm]	2.16	0.11
Volume [µL]	3.027	0.364

Mean and standard deviation (SD) of the measurements of individual drops on Sample 1 as reported in Table A1. Drop diameter is listed additionally.

Sample 2

Table A3

Drop	CA(m) [°]	CA(l) [°]	CA(r) [°]	Volume [µL]	Temperature [°C]
1	100.63	99.60	101.66	3.249	23.6
2	87.24	89.00	85.49	3.493	23.5
3	93.37	93.55	93.19	3.240	23.5
4	92.62	94.04	91.19	3.236	23.5
5	102.74	103.26	102.21	3.293	23.6
6	101.08	101.61	100.56	-	23.7

Measurements of contact angles on Sample 2 for six different drops. CA(l), CA(r): contact angles on the left and right side of the drop, respectively, as seen in the microscope. CA(m): Mean of CA(l) and CA(r). The volume of the drops and the ambient air temperature at the time of the placement of the drop on the surface are also listed.

Table A4

Measured Entity	Mean	SD
CA(m) [°]	96.28	6.12
CA(l) [°]	96.85	5.51
CA(r) [°]	95.72	6.82
Temperature [°C]	23.6	0.1
Diameter [mm]	2.23	0.13
Volume [µL]	3.302	0.109

Mean and standard deviation (SD) of the measurements of individual drops on Sample 2 as reported in Table A3. Drop diameter is listed additionally.

Sample 3

Table A5

Drop	CA(m) [°]	CA(l) [°]	CA(r) [°]	Volume [µL]	Temperature [°C]
1	111.90	112.33	111.47	3.060	23.3
2	113.06	113.12	113.00	3.152	23.4
3	104.69	104.35	105.04	2.893	23.4
4	100.57	100.52	100.62	3.150	23.4
5	97.39	97.31	97.46	2.956	23.4
6	108.55	109.02	108.08	2.678	23.5
7	91.02	91.05	90.98	3.097	23.5

Measurements of contact angles on Sample 3 for seven different drops. CA(l), CA(r): contact angles on the left and right side of the drop, respectively, as seen in the microscope. CA(m): Mean of CA(l) and CA(r). The volume of the drops and the ambient air temperature at the time of the placement of the drop on the surface are also listed.

Table A6

Measured Entity	Mean	SD
CA(m) [°]	103.88	8.06
CA(l) [°]	103.96	8.19
CA(r) [°]	103.81	7.94
Temperature [°C]	23.4	0.1
Diameter [mm]	2.01	0.17
Volume [µL]	2.998	0.171

Mean and standard deviation (SD) of the measurements of individual drops on Sample 3 as reported in Table A5. Drop diameter is listed additionally.

Sample 4

Table A7

Drop	CA(m) [°]	CA(l) [°]	CA(r) [°]	Volume [µL]	Temperature [°C]
1	79.55	76.74	82.35	-	23.8
2	92.29	91.72	92.86	-	23.8
3	87.96	90.38	85.54	-	23.8
4	99.15	98.61	99.70	-	23.8
5	106.36	106.64	106.08	-	23.8
6	95.34	95.06	95.61	-	23.8
7	91.20	92.38	90.01	-	23.8

Measurements of contact angles on Sample 2 for six different drops. CA(l), CA(r): contact angles on the left and right side of the drop, respectively, as seen in the microscope. CA(m): Mean of CA(l) and CA(r). The ambient air temperature at the time of the placement of the drop on the surface is also listed. The volume of the drops was not measured in this sample because of a device error.

Table A8

Measured Entity	Mean	SD
CA(m) [°]	93.12	8.48
CA(l) [°]	93.08	9.08
CA(r) [°]	93.16	8.17
Temperature [°C]	23.8	0
Diameter [mm]	-	-
Volume [µL]	-	-

Mean and standard deviation (SD) of the measurements of individual drops on Sample 4 as reported in Table A7.

Sample 5

Table A9

Drop	CA(m) [°]	CA(l) [°]	CA(r) [°]	Volume [µL]	Temperature [°C]
1	86.21	85.25	87.16	3.157	23.9
2	76.00	77.38	74.63	3.462	23.9
3	83.32	80.97	85.67	3.384	23.9
4	75.43	77.01	73.84	3.348	23.8
5	75.82	75.26	76.38	3.139	23.9
6	89.85	89.61	90.09	3.240	23.9
7	92.17	92.79	91.55	3.252	23.9

Measurements of contact angles on Sample 5 for seven different drops. CA(l), CA(r): contact angles on the left and right side of the drop, respectively, as seen in the microscope. CA(m): Mean of CA(l) and CA(r). The volume of the drops and the ambient air temperature at the time of the placement of the drop on the surface are also listed.

Table A10

Measured Entity	Mean	SD
CA(m) [°]	82.68	7.05
CA(l) [°]	82.61	6.77
CA(r) [°]	82.76	7.58
Temperature [°C]	23.9	0
Diameter [mm]	2.47	0.14
Volume [µL]	3.283	0.12

Mean and standard deviation (SD) of the measurements of individual drops on Sample 5 as reported in Table A9. Drop diameter is listed additionally.

Sample 6

Table A11

Drop	CA(m) [°]	CA(l) [°]	CA(r) [°]	Volume [µL]	Temperature [°C]
1	59.92	61.41	58.43	3.099	24.0
2	52.42	53.14	51.69	2.825	24.0
3	47.92	48.95	46.89	2.723	24.1
4	52.14	53.31	50.97	2.870	24.0
5	50.77	51.41	50.13	2.783	24.0
6	49.61	49.34	49.88	3.042	24.0
7	44.74	45.88	43.60	2.645	24.0

Measurements of contact angles on Sample 6 for seven different drops. CA(l), CA(r): contact angles on the left and right side of the drop, respectively, as seen in the microscope. CA(m): Mean of CA(l) and CA(r). The volume of the drops and the ambient air temperature at the time of the placement of the drop on the surface are also listed.

Table A12

Measured Entity	Mean	SD
CA(m) [°]	51.07	4.72
CA(l) [°]	51.92	4.93
CA(r) [°]	50.23	4.57
Temperature [°C]	24	0
Diameter [mm]	3.08	0.07
Volume [µL]	2.855	0.165

Mean and standard deviation (SD) of the measurements of individual drops on Sample 6 as reported in Table A11. Drop diameter is listed additionally.

Sample 7

Table A13

Drop	CA(m) [°]	CA(l) [°]	CA(r) [°]	Volume [µL]	Temperature [°C]
1	36.12	34.94	37.31	3.325	23.9
2	32.94	33.28	32.61	3.492	24.2
3	42.58	43.38	41.79	3.056	24.1
4	42.86	41.75	43.97	2.812	24.1
5	42.12	41.81	42.44	3.291	24.1
6	37.40	34.68	40.11	4.042	24.1
7	42.22	48.42	36.02	3.105	23.9

Measurements of contact angles on Sample 7 for seven different drops. CA(l), CA(r): contact angles on the left and right side of the drop, respectively, as seen in the microscope. CA(m): Mean of CA(l) and CA(r). The volume of the drops and the ambient air temperature at the time of the placement of the drop on the surface are also listed.

Table A14

Measured Entity	Mean	SD
CA(m) [°]	39.46	3.96
CA(l) [°]	39.75	5.59
CA(r) [°]	39.18	4.04
Temperature [°C]	24	0.1
Diameter [mm]	3.59	0.24
Volume [µL]	3.303	0.392

Mean and standard deviation (SD) of the measurements of individual drops on Sample 7 as reported in Table A14. Drop diameter is listed additionally.

Sample 8

Table A15

Drop	CA(m) [°]	CA(l) [°]	CA(r) [°]	Volume [µL]	Temperature [°C]
1	32.80	30.81	34.80	3.723	24.2
2	35.86	37.97	33.75	3.240	24.2
3	31.31	32.83	29.78	3.502	24.2
4	34.90	25.94	43.85	4.283	24.0
5	19.76	18.93	20.58	3.155	24.0
6	33.66	33.40	33.92	3.249	24.1
7	30.85	30.12	31.59	3.259	24.1

Measurements of contact angles on Sample 8 for seven different drops. CA(l), CA(r): contact angles on the left and right side of the drop, respectively, as seen in the microscope. CA(m): Mean of CA(l) and CA(r). The volume of the drops and the ambient air temperature at the time of the placement of the drop on the surface are also listed.

Table A16

Measured Entity	Mean	SD
CA(m) [°]	31.3	5.4
CA(l) [°]	30	6.09
CA(r) [°]	32.61	6.93
Temperature [°C]	24.1	0.1
Diameter [mm]	4.07	0.34
Volume [µL]	3.487	0.402

Mean and standard deviation (SD) of the measurements of individual drops on Sample 8 as reported in Table A15. Drop diameter is listed additionally.

Sample 9

Table A17

Drop	CA(m) [°]	CA(l) [°]	CA(r) [°]	Volume [µL]	Temperature [°C]
1	76.92	76.02	77.82	3.194	24.1
2	72.15	72.31	71.99	3.473	24.1
3	78.93	79.11	78.75	2.809	24.1
4	95.53	96.00	95.05	3.050	24.1
5	77.90	78.51	77.30	3.411	24.1
6	81.09	80.74	81.43	3.567	24.1
7	91.42	90.49	92.34	3.389	24.1

Measurements of contact angles on Sample 9 for seven different drops. CA(l), CA(r): contact angles on the left and right side of the drop, respectively, as seen in the microscope. CA(m): Mean of CA(l) and CA(r). The volume of the drops and the ambient air temperature at the time of the placement of the drop on the surface are also listed.

Table A18

Measured Entity	Mean	SD
CA(m) [°]	81.99	8.38
CA(l) [°]	81.88	8.37
CA(r) [°]	82.1	8.44
Temperature [°C]	24.1	0
Diameter [mm]	2.5	0.2
Volume [µL]	3.27	0.268

Mean and standard deviation (SD) of the measurements of individual drops on Sample 9 as reported in Table A17. Drop diameter is listed additionally.

Sample 10

Table A19

Drop	CA(m) [°]	CA(l) [°]	CA(r) [°]	Volume [µL]	Temperature [°C]
1	102.09	102.21	101.97	2.714	24.2
2	95.71	96.10	95.32	3.156	24.3
3	105.73	105.26	106.21	3.436	24.2
4	110.40	111.41	109.38	3.105	24.1
5	110.80	110.84	110.75	2.818	24.1
6	103.06	103.06	103.05	3.054	24.1
7	108.47	107.72	109.21	3.234	24.1

Measurements of contact angles on Sample 10 for seven different drops. CA(l), CA(r): contact angles on the left and right side of the drop, respectively, as seen in the microscope. CA(m): Mean of CA(l) and CA(r). The volume of the drops and the ambient air temperature at the time of the placement of the drop on the surface are also listed.

Table A20

Measured Entity	Mean	SD
CA(m) [°]	105.18	5.38
CA(l) [°]	105.23	5.37
CA(r) [°]	105.13	5.45
Temperature [°C]	24.2	0.1
Diameter [mm]	2	0.12
Volume [µL]	3.074	0.245

Mean and standard deviation (SD) of the measurements of individual drops on Sample 10 as reported in Table A20. Drop diameter is listed additionally.

Sample 11

Table A21

Drop	CA(m) [°]	CA(l) [°]	CA(r) [°]	Volume [µL]	Temperature [°C]
1	84.23	83.14	85.31	3.514	24.4
2	84.82	85.00	84.64	3.188	24.3
3	91.04	90.46	91.62	3.540	24.3
4	95.02	94.48	95.56	3.451	24.3
5	97.64	97.83	97.46	3.194	24.2
6	94.85	95.81	93.90	3.300	24.2
7	87.87	87.50	88.23	3.779	24.2

Measurements of contact angles on Sample 11 for seven different drops. CA(l), CA(r): contact angles on the left and right side of the drop, respectively, as seen in the microscope. CA(m): Mean of CA(l) and CA(r). The volume of the drops and the ambient air temperature at the time of the placement of the drop on the surface are also listed.

Table A22

Measured Entity	Mean	SD
CA(m) [°]	90.78	5.3
CA(l) [°]	90.6	5.64
CA(r) [°]	90.96	5.03
Temperature [°C]	24.3	0.1
Diameter [mm]	2.36	0.13
Volume [µL]	3.424	0.213

Mean and standard deviation (SD) of the measurements of individual drops on Sample 11 as reported in Table A21. Drop diameter is listed additionally.

Samples 12 to 17

Samples 12, 13, 14, 15, 16, and 17 were par of an experimental series that was discontinued due to sample damage by mechanical impact. This series was thus not included in the reported results.

Sample 18

Table A23

Drop	CA(m) [°]	CA(l) [°]	CA(r) [°]	Volume [µL]	Temperature [°C]
1	65.62	64.94	66.29	2.825	24.4
2	47.82	46.48	49.17	3.598	24.3
3	49.54	49.87	49.22	3.408	24.4

Measurements of contact angles on Sample 18 for three different drops. CA(l), CA(r): contact angles on the left and right side of the drop, respectively, as seen in the microscope. CA(m): Mean of CA(l) and CA(r). The volume of the drops and the ambient air temperature at the time of the placement of the drop on the surface are also listed.

Table A24

Measured Entity	Mean	SD
CA(m) [°]	54.33	9.81
CA(l) [°]	53.76	9.83
CA(r) [°]	54.89	9.87
Temperature [°C]	24.3	0
Diameter [mm]	3.13	0.36
Volume [µL]	3.277	0.403

Mean and standard deviation (SD) of the measurements of individual drops on Sample 18 as reported in Table A23. Drop diameter is listed additionally.

Sample 19

Table A25

Drop	CA(m) [°]	CA(l) [°]	CA(r) [°]	Volume [µL]	Temperature [°C]
1	61.70	61.80	61.61	3.390	24.4
2	54.32	54.30	54.35	3.250	24.4
3	59.33	59.48	59.17	3.695	24.5

Measurements of contact angles on Sample 19 for three different drops. CA(l), CA(r): contact angles on the left and right side of the drop, respectively, as seen in the microscope. CA(m): Mean of CA(l) and CA(r). The volume of the drops and the ambient air temperature at the time of the placement of the drop on the surface are also listed.

Table A26

Measured Entity	Mean	SD
CA(m) [°]	58.45	3.77
CA(l) [°]	58.53	3.84
CA(r) [°]	58.37	3.7
Temperature [°C]	24.4	0
Diameter [mm]	3.06	0.09
Volume [µL]	3.445	0.227

Mean and standard deviation (SD) of the measurements of individual drops on Sample 19 as reported in Table A25. Drop diameter is listed additionally.

Sample 20

Table A27

Drop	CA(m) [°]	CA(l) [°]	CA(r) [°]	Volume [µL]	Temperature [°C]
1	41.60	39.86	43.35	2.879	24.5
2	38.84	40.24	37.44	3.015	24.5
3	49.72	49.19	50.25	2.872	24.5

Measurements of contact angles on Sample 20 for three different drops. CA(l), CA(r): contact angles on the left and right side of the drop, respectively, as seen in the microscope. CA(m): Mean of CA(l) and CA(r). The volume of the drops and the ambient air temperature at the time of the placement of the drop on the surface are also listed.

Table A28

Measured Entity	Mean	SD
CA(m) [°]	43.39	5.66
CA(l) [°]	43.1	5.28
CA(r) [°]	43.68	6.41
Temperature [°C]	24.5	0
Diameter [mm]	3.31	0.23
Volume [µL]	2.922	0.081

Mean and standard deviation (SD) of the measurements of individual drops on Sample 20 as reported in Table A27. Drop diameter is listed additionally.

Sample 21

Table A29

Drop	CA(m) [°]	CA(l) [°]	CA(r) [°]	Volume [µL]	Temperature [°C]
1	43.50	44.85	42.15	1.362	24.4
2	30.69	27.93	33.44	2.635	24.5
3	54.24	56.31	52.18	3.003	24.5
4	60.56	63.88	57.23	3.004	24.3
5	41.78	34.54	49.01	3.137	24.4

Measurements of contact angles on Sample 21 for five different drops. CA(l), CA(r): contact angles on the left and right side of the drop, respectively, as seen in the microscope. CA(m): Mean of CA(l) and CA(r). The volume of the drops and the ambient air temperature at the time of the placement of the drop on the surface are also listed.

Table A30

Measured Entity	Mean	SD
CA(m) [°]	46.15	11.6
CA(l) [°]	45.5	14.86
CA(r) [°]	46.8	9.26
Temperature [°C]	24.4	0.1
Diameter [mm]	3.1	0.43
Volume [µL]	2.628	0.732

Mean and standard deviation (SD) of the measurements of individual drops on Sample 21 as reported in Table A30. Drop diameter is listed additionally.

Control A

Control A was replaced by replaced by Control B, because Control A was contaminated by improper handling.

Control B

Table A31

Drop	CA(m) [°]	CA(l) [°]	CA(r) [°]	Volume [µL]	Temperature [°C]
1	51.72	51.55	51.88	3.069	24.5
2	54.23	53.36	55.10	3.093	24.5
3	54.51	53.57	55.45	3.305	24.4

Measurements of contact angles on Control B for three different drops. CA(l), CA(r): contact angles on the left and right side of the drop, respectively, as seen in the microscope. CA(m): Mean of CA(l) and CA(r). The volume of the drops and the ambient air temperature at the time of the placement of the drop on the surface are also listed.

Table A32

Measured Entity	Mean	SD
CA(m) [°]	53.49	1.54
CA(l) [°]	52.83	1.11
CA(r) [°]	54.14	1.97
Temperature [°C]	24.4	0
Diameter [mm]	3.12	0.02
Volume [µL]	3.156	0.13

Mean and standard deviation (SD) of the measurements of individual drops on Control B as reported in Table A31. Drop diameter is listed additionally.

Control C

Table A33

Drop	CA(m) [°]	CA(l) [°]	CA(r) [°]	Volume [µL]	Temperature [°C]
1	95.17	94.58	95.77	2.361	24.4
2	90.96	91.59	90.33	3.700	24.4
3	75.57	74.77	76.37	3.344	24.4

Measurements of contact angles on Control C for three different drops. CA(l), CA(r): contact angles on the left and right side of the drop, respectively, as seen in the microscope. CA(m): Mean of CA(l) and CA(r). The volume of the drops and the ambient air temperature at the time of the placement of the drop on the surface are also listed.

Table A34

Measured Entity	Mean	SD
CA(m) [°]	87.23	10.32
CA(l) [°]	86.98	10.68
CA(r) [°]	87.49	10.01
Temperature [°C]	24.4	0
Diameter [mm]	2.34	0.32
Volume [µL]	3.135	0.694

Mean and standard deviation (SD) of the measurements of individual drops on Control C as reported in Table A33. Drop diameter is listed additionally.

SURFACE ANALYSIS

The surface roughness of the samples was analysed using laser scanning microscopy. Surface roughness is reported in Table 10 and surface renderings of some samples and controls are shown in Figs. 20 to 23. For comparison, surface renderings of the original griddle are depicted here below at two different magnifications.

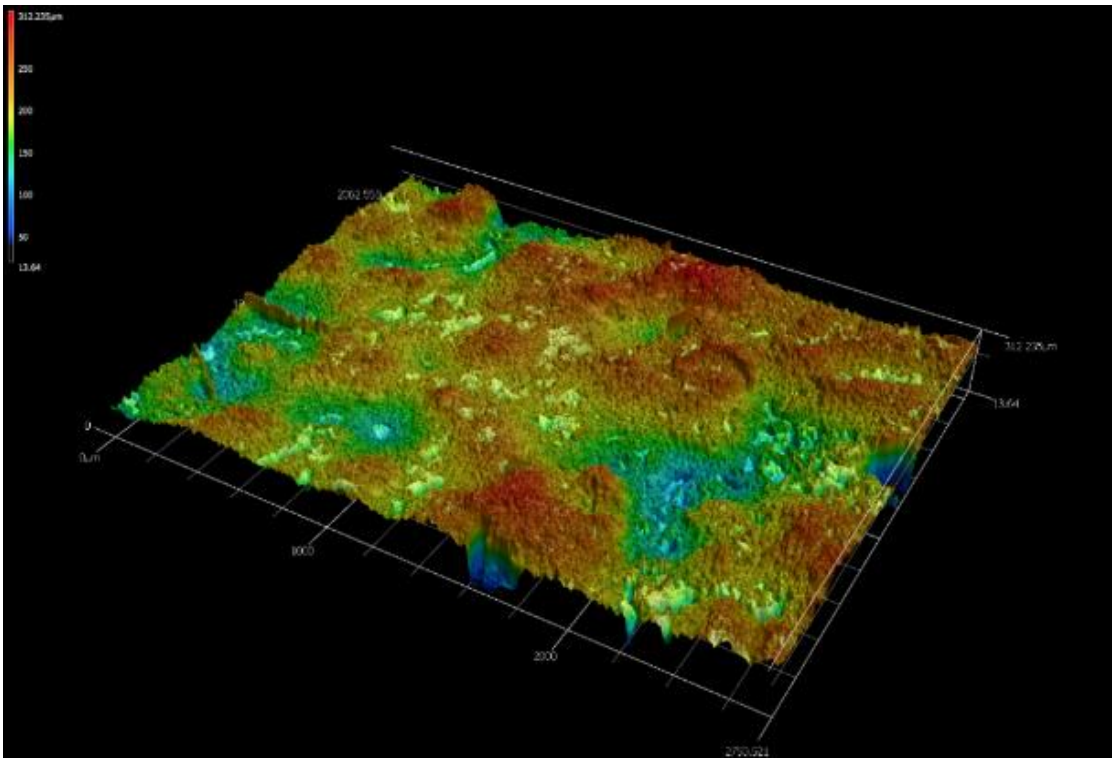

Fig. A1: 3D-map of a sample with the griddles original surface taken using a Keyence VK-X100 series laser scanning microscope at 5x magnification.

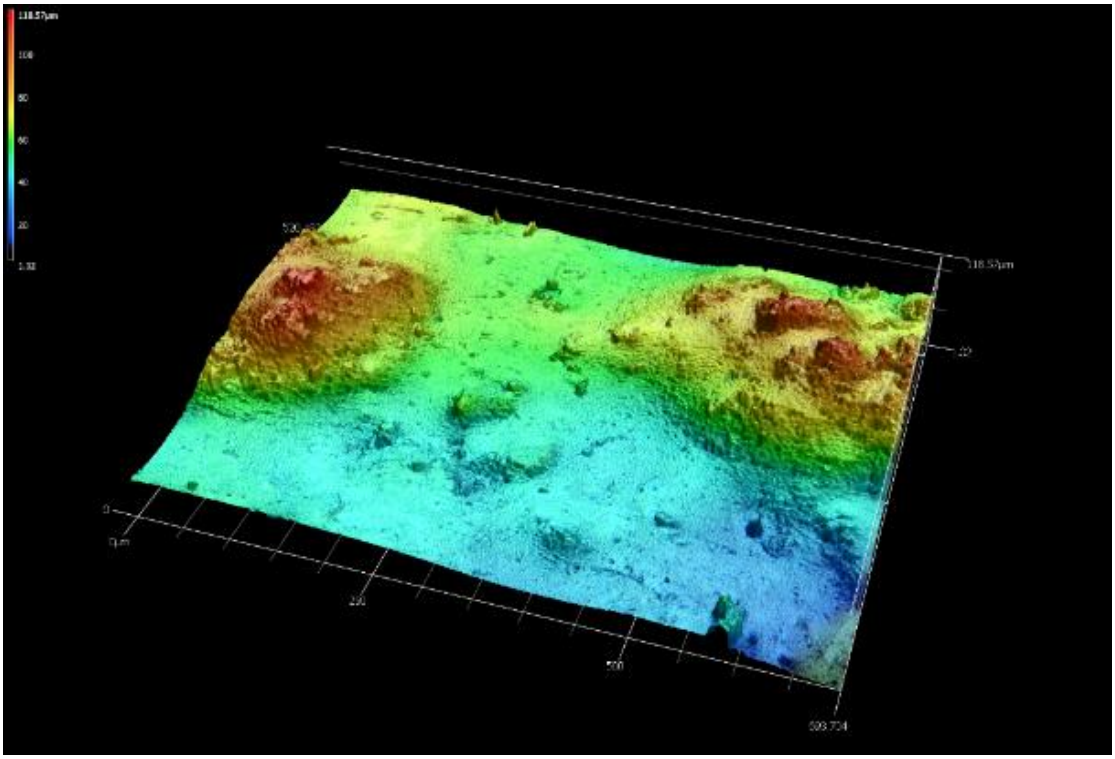

Fig. A2: 3D-map of a sample with the griddles original surface taken using a Keyence VK-X100 series laser scanning microscope at 20x magnification.